Embedded physical constraints in machine learning to enhance vegetation phenology prediction

Mengying Cao & Qihao Weng

View supplementary material

Published online: 26 Nov 2024.

Submit your article to this journal

Article views: 1070

View related articles

View Crossmark data

Taylor & Francis
Taylor & Francis Group

Embedded physical constraints in machine learning to enhance vegetation phenology prediction

Mengying Cao[a,b] and Qihao Weng [ID][a,b,c]

[a]JC STEM Lab of Earth Observations, Department of Land Surveying and Geo-Informatics, The Hong Kong Polytechnic University, Hung Hom, Hong Kong; [b]Research Centre for Artificial Intelligence in Geomatics, The Hong Kong Polytechnic University, Hung Hom, Hong Kong; [c]Research Institute for Land and Space, The Hong Kong Polytechnic University, Hung Hom, Hong Kong

ABSTRACT

Vegetation phenology plays a pivotal role in ecological processes on terrestrial surfaces and the interactions between the biosphere and atmospheric feedback. Current attempts to retrieve vegetation phenology have primarily depended on vegetation indices extracted from satellite remote sensing imagery. These approaches often neglect the underlying physical mechanisms associated with climatic factors, and there is a notable absence of evaluations and comparisons with field-observed phenology inventory data. To address these limitations, this paper proposes an innovative physical constraint neural networks (PCNNs) model that combines machine learning techniques with physical mechanisms to enhance the accuracy of vegetation phenology predictions. By incorporating meteorological variables into a machine learning model and by using the Moderate-Resolution Imaging Spectroradiometer (MODIS) dataset to identify the vegetation phenology of four vegetation types in North America, this study delved into the relationship between vegetation phenology and climate factors as well as its impacts on ecosystems. Our model demonstrated high accuracy compared to machine learning methods without physical mechanisms when validated by field observations from PhenoCam and the USA National Phenology Network (USA-NPN) spanning from 2001 to 2021. The results show that the overall root mean square error (RMSE) with physical constraints is reduced to 12.37 days, higher by 2.6 days than the machine learning method without physical constraints. We compared four vegetation types using different machine learning and traditional rule-based methods, deciduous vegetation (DV) exhibited the most favorable prediction results, with the RMSE and mean bias error (MBE) as low as 5.71 days and 4.06 days in PCNNs model, respectively. This was followed by evergreen needle-leaved forests and mixed forests with RMSE of 12.32 and 13.28 days, respectively. The stressed deciduous vegetation type had the worst prediction result of 19.86 days (RMSE), and the weighted index of agreement (WIA) attained a value of 0.68. These findings suggest that the model embedded with physical constraints significantly boosted prediction accuracy for four common vegetation types, particularly for DV, compared to the unconstrained ML model. It offers valuable insights into the incorporation of physical mechanisms within machine learning models. This research paves the way for substantial advancements in the field of land surface phenology, enabling more accurate and reliable predictions of vegetation phenology in various ecological and climatic contexts.

1. Introduction

Vegetation phenology refers to the study of the specific timing and recurring patterns of vegetation lifecycle events, which are often triggered by environmental factors. The processes of vegetation phenology have been characterized by a series of key events in plant life, such as leaf unfolding, senescence, and dormancy (Cheng et al. 2020; Parihar et al. 2013; Stöckli et al. 2011; Zeng et al. 2020). These phenomena are tightly interwoven with biogeochemical processes such as photosynthesis, transpiration and carbon cycling, which have an impact on the delicate balance of energy between the surface and the atmosphere (Verhegghen, Bontemps, and Defourny 2014; Zeng et al. 2020). The impact of global climate change on vegetation phenology directly influences the energy balance of ecosystems and their capacity for feedback regulation. Therefore, a thorough investigation of vegetation phenology will not only help us to better understand the functioning of ecosystems but also provide a scientific basis for addressing global

CONTACT Qihao Weng ✉ qihao.weng@polyu.edu.hk

climate change and promoting sustainable development.

The variation in vegetation phenology serves as a sensitive indicator of the impact of seasonal and climate fluctuations on vegetation, highlighting its significance as a crucial metric for assessing ecological responses to changing climatic conditions (Seyednasrollah et al. 2019). Numerous methods exist to detect the variations in vegetation phenology, including human visual assessment, near-surface measurement and satellite remote sensing. These approaches provide insight into physiological and biochemical processes at different stages of vegetation development. Traditional vegetation monitoring relies on human perception of changes in vegetation characteristics (Elmendorf et al. 2016; McDonough MacKenzie, Gallinat, and Zipf 2020; Parihar et al. 2013), limited by labor availability but crucial for calibrating and validating vegetation phenology models (Liang, Schwartz, and Fei 2011; Purdy et al. 2023; Zhao, Donnelly, and Schwartz 2020). Field-observed methods can be applied across various spatial scales, from individual plants to large-scale landscapes (Park, Newman, and Breckheimer 2021; Piao et al. 2019). Many observational networks, such as the Pan European Phenology Network (PEPN) (Templ et al. 2018; Tian et al. 2021) and the USA National Phenology Network (USA-NPN), have been used for vegetation phenology validation of satellite remote sensing data methods (Peng et al. 2017; Xin et al. 2020). Near-surface measurements have proven to be a valuable data source for conducting phenological studies, enabling near real-time monitoring of vegetation phenology (Cao et al. 2021; Hufkens et al. 2012). For instance, PhenoCam has been a popular tool for exploring vegetation phenology in recent years and can provide high-frequency and high-spatial resolution near-surface data (Klosterman et al. 2014; Seyednasrollah et al. 2019). The inception of satellite remote sensing technologies armed with advanced sensors capable of discerning a broad spectrum of light wavelengths has empowered these satellite platforms to conduct holistic surveillance of vegetation dynamics (Melaas, Friedl, and Zhu 2013; Zhang et al. 2004; Zhou et al. 2016). The quintessential advantage of this technological innovation lies in its provision of wide-ranging spatial coverage coupled with unparalleled temporal resolution, attributes that are quintessential for the precise anticipation of ecosystemic adaptations to environmental fluxes.

The application of remote sensing data, through the exploitation of vegetation indices such as the normalized difference vegetation index (NDVI) (Lüdeke, Ramage, and Kohlmaier 1996; Touhami et al. 2022), leaf area index (LAI) (Fang et al. 2019), enhanced vegetation index (EVI) (Verhegghen, Bontemps, and Defourny 2014), and two-band enhanced vegetation index (EVI2) (Caparros-Santiago, Rodriguez-Galiano, and Dash 2021; Jiang et al. 2008) has become instrumental in the precise and dependable forecasting of phenological alterations. EVI2 is highly esteemed for its superior accuracy compared to similar counterparts due to its reduced susceptibility to the influence of background soil albedo (Wu et al. 2021; Zeng et al. 2020). These spectral indicators are pivotal for delineating subtle inter-annual variations in vegetation, thereby facilitating the construction of predictive models. Among these commonly employed metrics included the start of season (SOS), end of season (EOS), peak of season (POS), and the length of the growing season (GSL), all of which are derived from spectral remote sensing observations (De Beurs and Henebry 2010; Gao et al. 2023; Zhang et al. 2003).

Machine learning (ML) techniques have emerged as a formidable tool in the modeling and prediction of human-environment interactions, particularly through the application of remote sensing data. These techniques have been extensively utilized to assess vegetation phenology across diverse terrestrial ecosystems at varying scales, which has the advantage of efficiently identifying vegetation phenology directly from images without the time series (Cao et al. 2021; Xin et al. 2020; Zhou et al. 2021). Despite the notable benefits of ML, such conventional methodologies often fail to account for the essential physical mechanisms that underlie phenological processes. A critical limitation of traditional ML approaches is that vegetation phenology does not consider the effects of complex biophysical-chemical processes (e.g. photosynthesis) of vegetation phenology (Li et al. 2024; Wang, Zhang, and Rodman 2021; Xin et al. 2020). Non-machine learning modeling approaches consider simple physical processes (Sun et al. 2019; Turner, Ollinger, and Kimball 2004; Wang et al. 2023), but they are also limited to focusing on a few factors and have not yet been integrated into ML frameworks (Shen et al. 2011; Tian et al. 2024). Therefore, there is an urgent need to develop the ML

method that can account for the physical constraints inherent in ecosystems, enabling more accurate predictions of current vegetation phenology.

To further improve prediction accuracy and understand the physical mechanisms of vegetation phenology, it is necessary to incorporate the physical constraints into the ML model for vegetation phenology. Recent advancements have witnessed the burgeoning application of embedding physical constraints within ML frameworks in other domains, such as engineering (Mohan et al. 2020; Zang et al. 2021), chemistry (Prezhdo 2020), agriculture (Guo et al. 2021) and climate detection (Lin et al. 2023; Yan et al. 2024). This approach has been verified not only improves their performance but also enhances their interpretability (Cuomo et al. 2022; Zhang et al. 2022). By integrating physical constraints, such as the effects of temperature, precipitation, and solar radiation, we can enhance the accuracy and reliability of vegetation phenology predictions. These constraints provide valuable contextual information that captures the underlying processes governing plant growth and development. By leveraging large amounts of data and powerful algorithms, ML models can capture complex relationships and patterns between environmental factors and vegetation growth processes, which can lead to more accurate and reliable predictions.

This research aims to develop physical constraint neural networks (PCNNs) to enhance the prediction of vegetation phenology. The model will incorporate physical constraints, which include energy balance mechanisms, ecological niche theory, and biophysical principles. By exploring the inclusion of physical constraints into the machine learning framework, we seek to improve the accuracy, robustness, and generalizability of machine learning models in capturing the intricate dynamics of vegetation phenology. To achieve our research objectives, we will leverage a diverse set of remote sensing data, including satellite imagery, climate data, and ground-based observations. The physically constrained model was compared the performances with those traditional rule-based and machine learning approaches to highlight the strengths of incorporating physical constraints. Overall, this study aims to bridge the gap between machine learning and ecological mechanisms understanding by demonstrating the importance of embedding physical constraints in machine learning models for vegetation phenology prediction. Consequently, we can unlock the full potential of machine learning techniques in advancing our knowledge of ecosystem dynamics and their response to environmental changes.

2. Study area and datasets

2.1. Study area

This study specifically focuses on North America, including countries like Canada, the United States of America, Mexico, Hawaii, and Puerto Rico. The geographical coordinates covered a wide range of latitudes in the Northern Hemisphere. According to the modified Köppen climate classification system, the North American region contains five broad climate classes spanning tropical climate to polar climate from south to north (Cui, Liang, and Wang 2021; Lohmann et al. 1993). Most vegetation in the study area was in the temperate and continental climate classes. These climate classes support a diverse array of land cover types (Nguyen et al. 2020; Peel, Finlayson, and McMahon 2007; Zhou et al. 2022). Tropical rainforest climate and tropical monsoon climate occupy a small portion in the study area, which are primarily composed of croplands, grasslands, and less mixed forests. While polar climate accounts for a larger proportion of the region, there is almost bare vegetation due to cold temperatures. The arid climate classes of this region are dominated by shrub lands and stressed deciduous vegetation (SDV). The temperate zones are primarily covered by deciduous vegetation (DV), grasslands, croplands, and shrub forests (SF). Continental regions are home to evergreen vegetation (EV) and SDV. The diverse climatic conditions within the study area have given rise to a high variety of vegetation types, allowing for the examination of the phenology of various vegetation types and the variability of their phenology patterns under different climate classes.

The land cover maps utilized in our study was derived from the MCD12Q1 dataset, which corresponds to the International Geosphere-Biosphere Programme (IGBP) classification system (Zhu and Woodcock 2014). The distribution of the main natural vegetation types in this region is shown in Figure 1. We selected four majors natural vegetation types: EV, DV, SF, and SDV. Cropland and grass are not
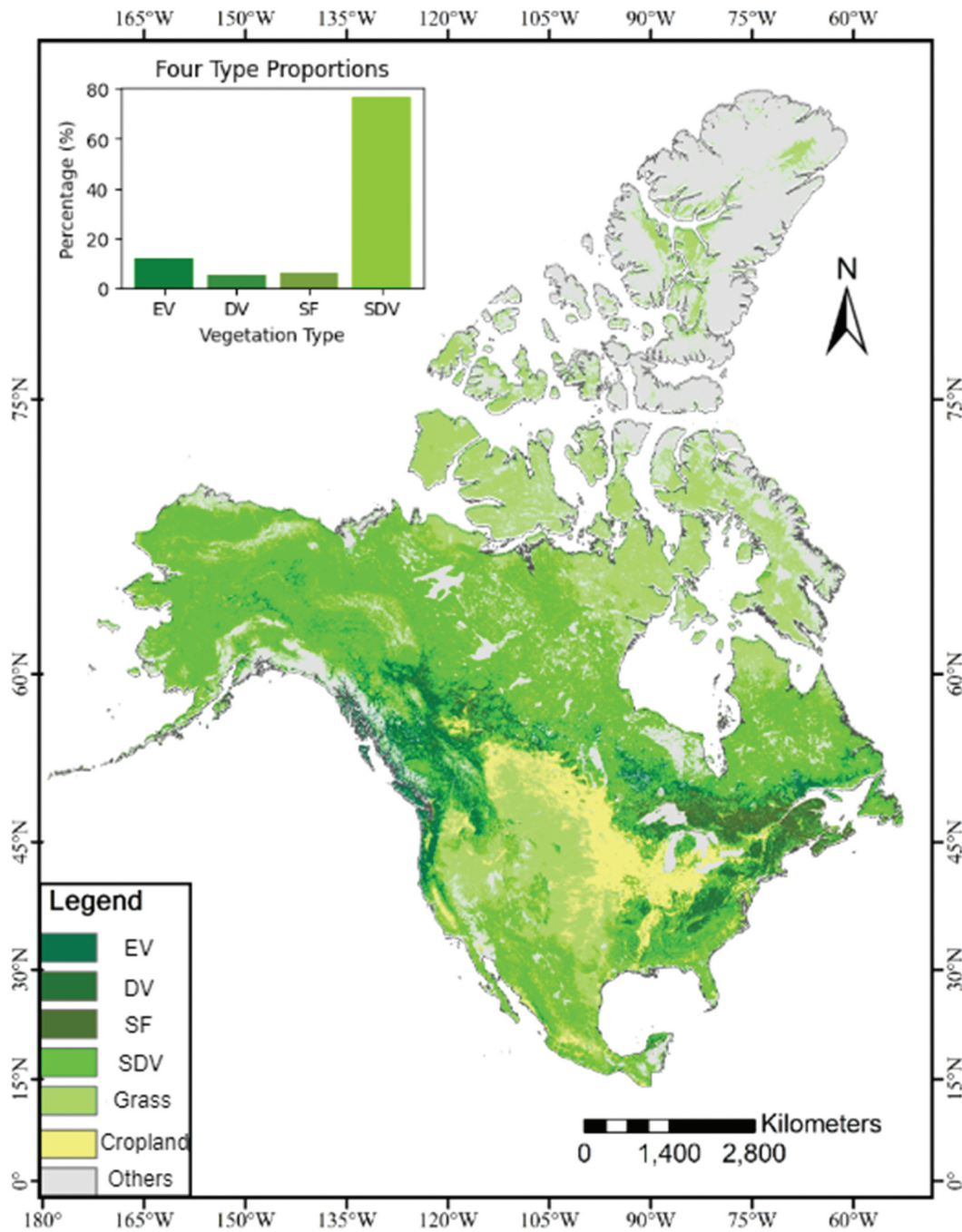
Figure 1. Distribution of the major natural vegetation covers in North America in 2019. The base map was obtained from the MCD12Q1 land cover product. The histogram figure indicates the percentage of the four vegetation types studied in the region. Note: EV: evergreen vegetation; DV: deciduous vegetation; SF: shrub forests; SDV: stressed deciduous vegetation; others: barren, water, or snow/ice.

considered in this study because they are more susceptible to human activities. EV is primarily represented by evergreen needle-leaved forests in this region, DV denotes deciduous broadleaf forests, SF includes open and closed shrublands, and SDV represents woody savannas or savannas. Grasslands and croplands are more likely to be impacted by humans,

so they are excluded from the scope of this study. Other non-vegetated land types, such as buildings and snow, were excluded from our analysis of vegetation phenology. The proportion of each of the four vegetation types varies within the study area. EV covered 12% of the total area, while DV occupied 5%. SF constituted 6% of the study area, whereas SDV

dominated with a substantial share of 77%. Moreover, the study region offers an abundant collection of field observation datasets for validation, coupled with enhanced spatial and temporal resolution of meteorological variables, thereby rendering it an optimal choice for exploring vegetation phenology. Our analysis will focus on these four vegetation types to explore their phenology and how they are influenced by the varying climates of North America.

2.2. Data acquisition

MOD09Q1 dataset: this dataset was derived from the MODIS sensor, which was mounted on NASA's Terra and Aqua satellites (Li et al. 2021; Tseng et al. 2019). This satellite dataset provided a comprehensive representation of the surface spectral reflectance, allowing us to analyze the vegetation indicator using different bands. These data were captured at a high resolution of 250 meters, ensuring precision and accuracy in their representation of the Earth's surface reflectance. For each pixel, a value was selected from all data collected during a periodic cycle of observations every 8 days. We selected MODIS data based on a series of criteria, including high observational coverage, a narrow viewing angle, low clouds or no cloud shadows, and low aerosol loading.

PhenoCam dataset: the PhenoCam network have been deployed cameras more than 800 sites for a wide range of vegetation types following the protocol in North America (Li et al. 2023; Seyednasrollah et al. 2019, Richardson et al. 2013). It has automatically recorded more than 4,900 site-years of data and these datasets are readily available for free access on the official platform (https://phenocam.nau.edu/web cam/about). This dataset contained three distinct types of observation sites on the website, designated Type I, Type II, and Type III. Type I adheres strictly to the standard protocol with active site personnel collaboration for maintenance. Type II has minor deviations but retains active site personnel involvement. Type III has deviations and lacks active site personnel collaboration (Seyednasrollah et al. 2019). To ensure high quality and minimize deviation, we select the Type I sites to validate vegetation phenology. For our study, we filtered high-quality data from Type I sites to validate vegetation phenology, excluding those affected by adverse weather conditions such

as rain, snow, and hail, as well as varying light conditions like clouds and aerosols. To ensure consistency and minimize the impact of sunlight scattering, we selected images captured at noon each day as our validation data. Based on PhenoCam data provided the vegetation types and the time series of vegetation index, we carefully selected four specific vegetation types from 56 sites that corresponded to the satellite data between 2010 and 2021. These vegetation types included deciduous broadleaf, evergreen conifer, shrubland, and tundra. The shrubland in the PhenoCam corresponded to SF in the satellite dataset, and tundra was categorized as SDV. According to our selection principle, the spatial distribution of this dataset was primarily concentrated within a latitudinal range of 32° to 57°N and at elevations reaching up to 1550 m. Appendix Table A1 presents the validation data of 851 site-years utilized in this study.

USA-NPN dataset: To further corroborate our prediction outcomes, we additionally employed field observation data derived from extensive datasets of the USA-NPN. This ground-based observation provided a detailed record of vegetation phenology events covering over 400 diverse plant types across approximately 3000 distinct sites (Bolton and Friedl 2013; Gao and Zhang 2021; Guo et al. 2021). We specifically selected all available records pertaining to the leaf category from 2007 to 2021 (table A2), encompassing a total of 4918 site-year datasets. These records cover a wide range of vegetation types, including deciduous broadleaf forests (1,726 records), evergreen coniferous forests (1,565 records), shrub forest (797 records), drought deciduous broadleaf and graminoid (1,430 records). To align the field-observed vegetation types with the specific vegetation categories derived from satellite remote sensing data, we assigned the vegetation type records of field-observed to the vegetation categories derived from satellite. The specific description for vegetation classification is shown in Table A3. Accordingly, shrub forest was classified as SF, while drought deciduous broadleaf and graminoid vegetation were classified as SDV. The initial growth of filed-observed corresponded to the SOS in satellite remote sensing, while the breaking leaf buds of filed-observed correspond to the EOS in satellite remote sensing. This categorization

allowed us to harmonize our data with the study's requirements, enabling a more accurate and relevant analysis of our prediction results.

Daymet datasets: this dataset provides daily, monthly and annual time-scale climate summaries spanning a long-term period from 1980 to the present (Thornton et al. 2022). We use the high-quality grided daymet datasets of daily climate variables at a 1 km resolution across North America, which offers a wealth of information on various meteorological parameters. In this study, we selected six meteorological variables that are most relevant to vegetation phenology as climatic factors based on previous studies (Meng et al. 2020; Touhami et al. 2022; Wang et al. 2022). The six meteorological variables of daymet gridded data are shown in Figure 2.

3. Methodology

This study aimed to identify vegetation phenology and investigate the underlying relationships and trends in North America from 2001 to 2021. To achieve this, a systematic processing flow consisting of three main steps was implemented. The specific process is illustrated in Figure 3.

3.1. Data preprocessing

MOD09Q1 was obtained and underwent a series of preprocessing steps. Data preprocessing was a fundamental step that ensured the quality and adequacy of the dataset for subsequent analytical endeavors. It played a crucial role in refining the raw data, correcting errors, and preparing the data for effective analysis. In this study, these steps included data cleaning, missing value imputation, outlier detection and removal, normalization, and feature selection.

After thoroughly cleaning and interpolating the raw dataset, we utilized the satellite dataset of red band (620 nm to 670 nm) and infrared band (841 nm to 876 nm) to compute the EVI2 from the MOD09Q1 datasets (Jiang et al. 2008; Zhang et al. 2022; Zhang et al. 2003). The vegetation index of EVI2 was able to obtain more accurate and informative insights into vegetation dynamics than other indices. As EVI2 was less susceptible to atmospheric conditions, making it a popular choice for monitoring vegetation dynamics and studying vegetation responses across various ecosystems (Helman 2018; Wu et al. 2021; Zeng et al. 2020). The value of EVI2 index ranged from −1 to 1, with higher values indicating healthier and more robust vegetation. This increased value was attributed to the absorption in the visible red
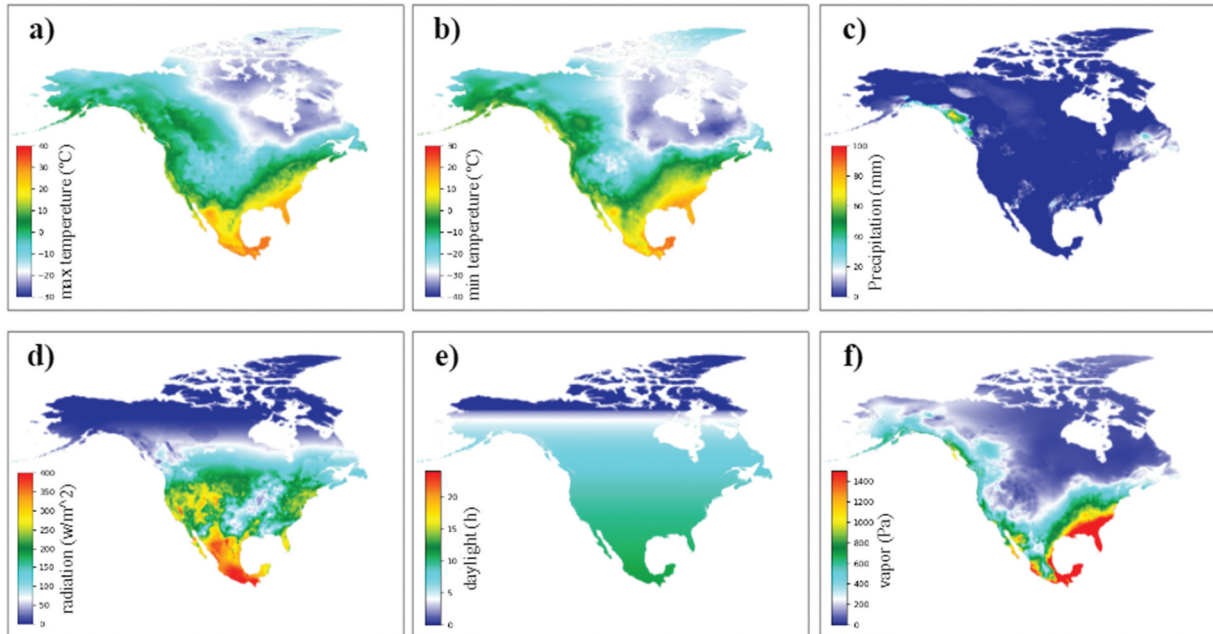

Figure 2. The six meteorological variables of daymet products for the year 2019. (a) daily average maximum 2-meter air temperature. (b) daily average minimum 2-meter air temperature. (c) daily total precipitation, (d) daily average shortwave radiation. (e) daily total duration of the daylight period, and (f) daily average partial pressure of water vapor.
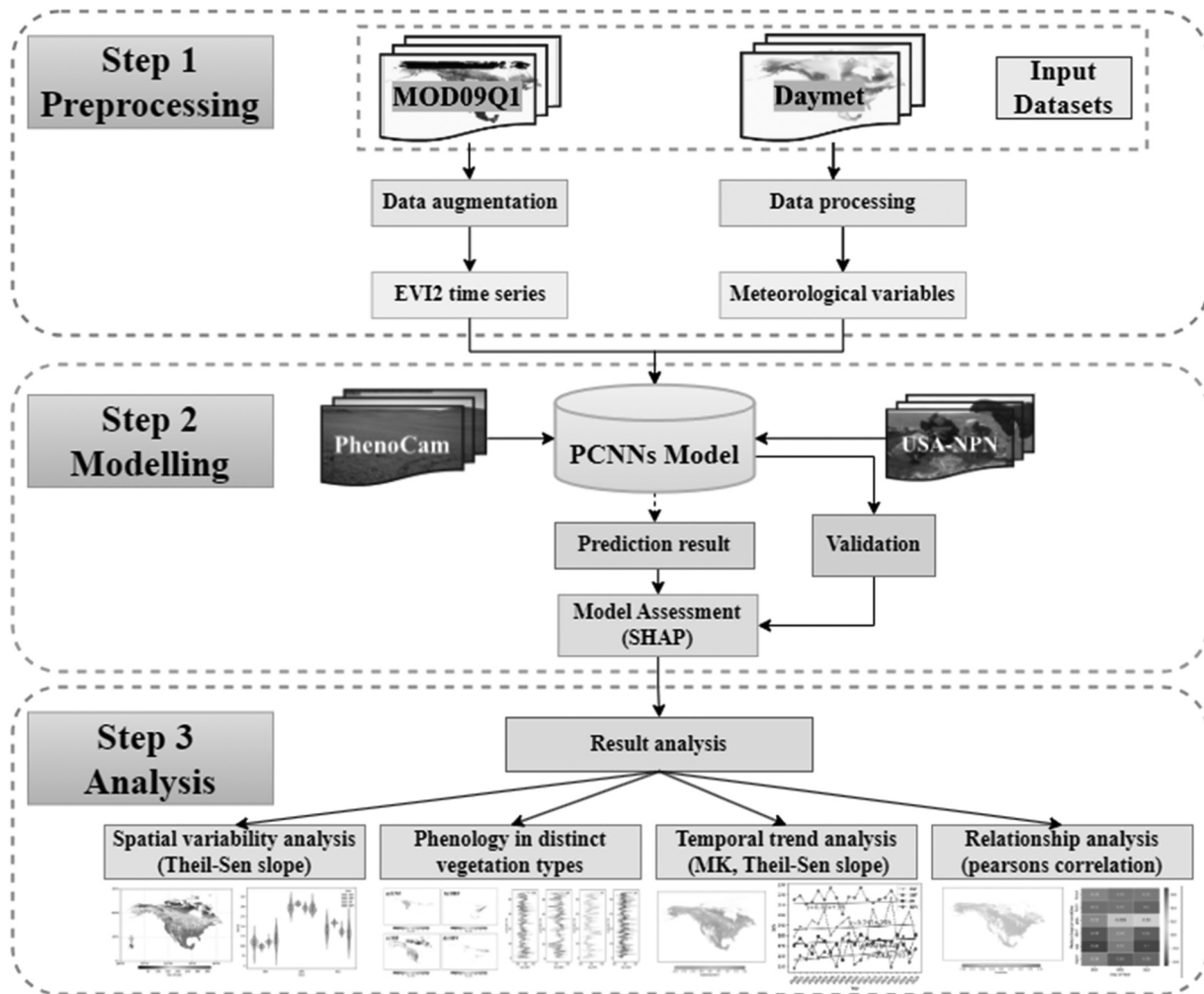
Figure 3. The flowchart for identifying vegetation phenology based on PCNNs model. Step 1 shows the preprocessing process of the input satellite data, which includes the satellite images augmentation and meteorological data transformation; step 2 displays the process of training and validation within the PCNNs model; and step 3 presents various relationship analysis related to the prediction results.

band of the electromagnetic spectrum, while low value denotes a tendency toward less or disappearing vegetation (Peng et al. 2021; Zhang et al. 2003). We employed an 8-day composite MODIS dataset with a 250-meter resolution to derive the EVI2 time series for each pixel. We replaced the data identified as snow with the closest snow-free data in the EVI2 time series and adopted the 7-point median moving method to fill up the cloudy or missing data. We identified outliers that differed from the median by more than three standard deviations in a 7-point moving window in the time series and replaced the identified outliers with the median in the moving window. In addition, we used the Savitzky-Golay (SG) filtering (Savitzky and Golay 1964) approach to smooth the EVI2 time series.

In this study, we selected 56 sites across North America for rigorous field validation of vegetation phenology. The PhenoCam platform generally provided a time series of green chromatic coordinates (GCC) that reflected a reliable seasonal trajectory of vegetation activity. The chromatic coordinates served as effective indicators, capturing the changes in vegetation throughout the year, from germination to senescence. In this study, we used the GCC index, which was conveniently available as a summary product on the PhenoCam website (Seyednasrollah et al. 2019). The PhenoCam dataset provides GCC values derived from the red, green, and blue bands. These values were calculated annually based on the percentage of the green band relative to the total RGB band for each pixel. To ensure the precision of our analysis,

we implemented stringent quality control measures on the GCC time series, encompassing filtering and outlier detection. Additionally, we visually examined the processed time series to detect any potential concerns. To address missing points in the GCC time series, we utilized a linear interpolation method, where we estimated the values based on adjacent points. The Savitzky – Golay smoothing algorithm was incorporated to eliminate the effect of cloud-related disturbances, which also effectively enhanced the accuracy of curve fitting. After the above steps, we

can effectively handle insufficient data and generate a more reliable display of the time series trend of GCC. Figure 4 presents the GCC time series of the four vegetation types, and their fitted curves (red color) are closely related to the leaf growth cycle. The SOS was determined as the precise date during the upward phase when the GCC first reaches 10% of the seasonal amplitude. This signified the initial day of leaf emergence in a particular year. The EOS was identified as the specific date during the declining phase when the GCC surpasses 90% of the seasonal
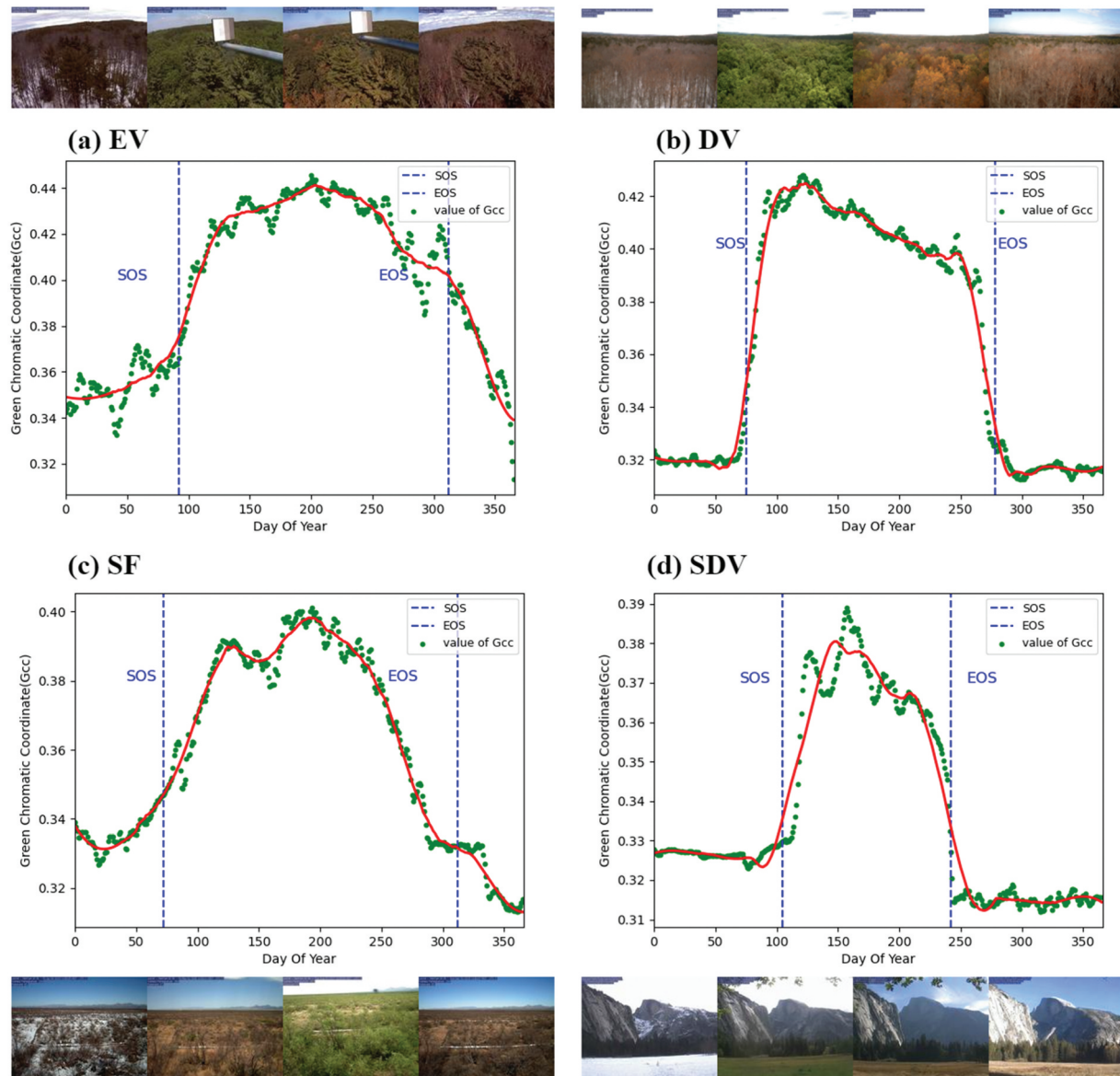
Figure 4. The time series of GCC for four vegetation types (EV: evergreen vegetation; DV: deciduous vegetation; SF: mixed forests; SDV: stressed deciduous vegetation) derived from the PhenoCam dataset in 2018. The red curve in this graph is the GCC fitting curve. (a) EV located in Harvardbarn2, (b) DV in Dukehw, (c) SF in ahwahnee, and (d) SDV in portal. The images of each site represent the four seasons and obtained from https://phenocam.nau.edu/webcam/sites/.

amplitude. This indicated the final growth date in the given year. The GLS was obtained by subtracting the EOS from the SOS for each year.

To validate the satellite-derived vegetation phenology predictions, we utilized ground-based phenology inventory from the USA-NPN. In these inventories, the spring phenological observations associated with remotely sensed SOS that were described as "initial growth," "breaking leaf buds" or "≥75% of full leaf size." During the autumn season, the EOS were described as "all/≥50% of leaves fallen," "all/≥50% of leaves colored." Moreover, we implemented a filtering process to exclude records that exhibited vegetation functional types that contradicted the MCD12Q1 land covers type within the designated data timeframe. Furthermore, we refined the vegetation date range using the day of year (DOY) metric. Specifically, for spring phenology, we limited the vegetation phenology within DOY 1 and DOY 200 in the study region. Similarly, for autumn phenology, we narrowed the range to DOY 150 and DOY 365. By restricting our analysis within these specified timeframes, we ensured a more precise assessment of vegetation dynamics during the relevant seasons.

In this study, we utilized daymet datasets aligned with the MODIS product covering the period from 2001 to 2021. From the daymet dataset, we carefully selected six meteorological variables that exhibited a strong correlation with phenology, particularly in the context of North America. These variables contained a range of meteorological factors, including maximum and minimum air temperatures, precipitation, daylight duration, radiation, and water vapor. The duration of the daylight period was measured in seconds throughout the day and then converted to hours to standardize the unit of measurement. This conversion ensures that the duration of daylight exposure can be easily compared and analyzed. Precipitation was meticulously recorded as the total amount accumulated over the course of a day, air temperature was recorded as the maximum and minimum values attained within a single day. Other climate variables were also converted to hours in a day to maintain consistency in the units of measurement. This standardization allows for a comprehensive and unified analysis of the various climatic factors that affect a given region or location. The six meteorological variables in the daymet dataset were calculated the mean value for each day of the year based on

each pixel. We resampled the daily daymet dataset to the same spatial resolution as the satellite dataset. After processing, the daily averages of these meteorological variables served as input datasets for further modeling, allowing for a thorough analysis of their relationships with vegetation phenology.

3.2. PCNNs model for vegetation phenology prediction

This study employed the physical constraint neural networks (PCNNs) to predict the vegetation phenology in North American phenology. The PCNNs could address the problem that experimental observations were described by few quantities or noisy points by using known data (Cuomo et al. 2022). In our study, the PCNNs model comprises five distinct components as shown in Figure 5 (Raissi, Perdikaris, and Karniadakis 2019). The input section primarily consists of satellite time series data and meteorological variables, the output part represents the predictions via the model. The deep neural network (DNN) component was utilized to extract key features and to determine precise parameters, while the physical constraints section serves to constrain the output results. In this process, the optimizer and loss function were operated in tandem to provide feedback to the model. After that, appropriate evaluation metrics were conducted to evaluate the model.

3.2.1. Neural network architecture

The models were trained using EVI2 time series and metrological variable datasets as the input datasets, and their performance was assessed using field-observed datasets such as the PhenoCam and USA-NPN datasets. To ensure the robustness and generalizability of the PCNNs model, a rigorous validation process was conducted using data augmentation. The deep neural network (DNN) component was utilized to extract feature values, specifically designed for extracting the features from the input datasets and outputting the preliminary results. It accomplished this by employing numerous layers of non-linear transformations to learn and extract feature representations. This part was adapted to different network layers or structures depending on the object to be extracted. This model could also apply to other networks, such as ANN or CNN to train this model, it depends on the requirement of prediction and the
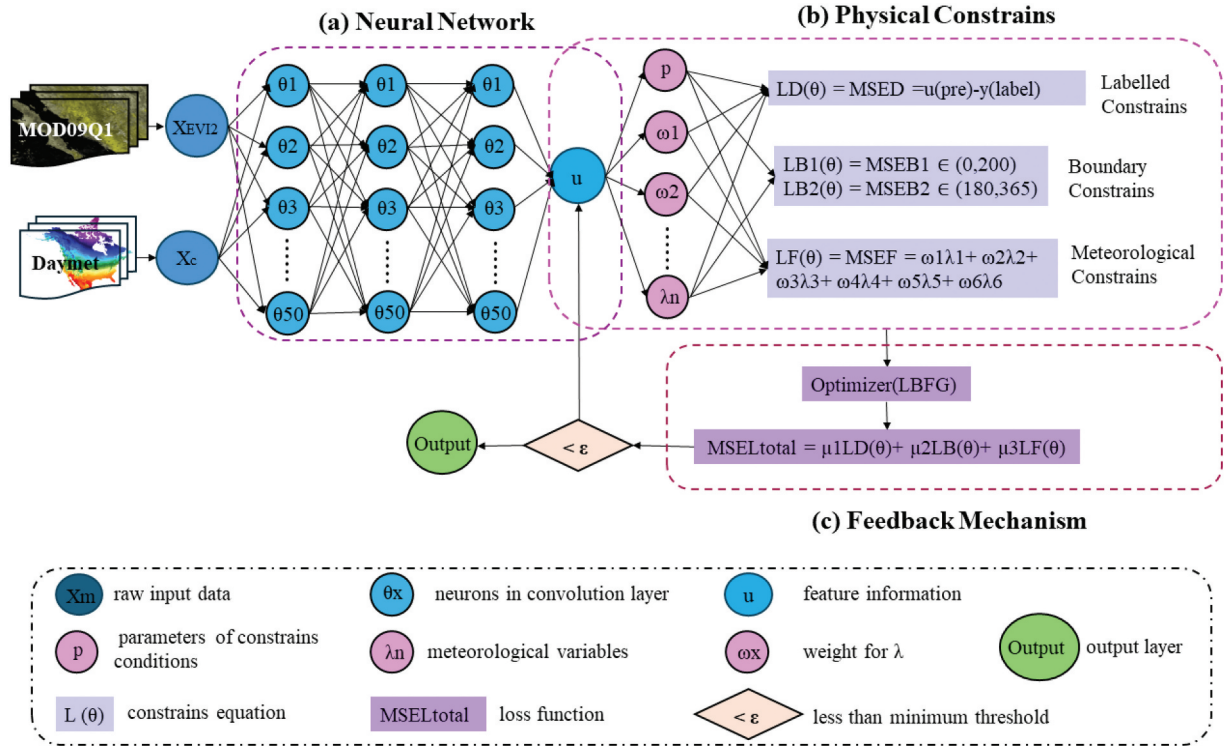
Figure 5. The architecture of physics-constrained neural networks for vegetation phenology prediction. (a) neural network that outputs the weight of each factor for the meteorological constraints, (b) physical constraints architecture for prediction, (c) feedback architecture.

features to be extracted. For this model, we experimented with the best choice of layers under ML using different layers (selected every 10 layers from 10 to 100). Then we determined that a 50-layer DNN was sufficient for feature extraction. The output model performance and number of layers are shown in Figure B1 The XEVI2 represented the input time series datasets, while Xc comprised a diverse set of six meteorological variables (maximum air temperature, minimum air temperature, precipitation, solar radiation, daylight duration and vapor pressure). Through an intricate process of image recognition, the advanced feature u was derived. The advance feature u is the derived result of the recognition on the image.

3.2.2. Physical constraints architecture

The physical constraints component was used for modifying and limiting the final result to suit the actual significance for the actual predictions, which was the innovative core of the model (Cuomo et al. 2022). In the physical constraints stage, we employed a range of constraints for the model, including boundary constraints, labeled constraints, and meteorological

constraints. The labeled constraints were utilized to adjust the prediction results. The boundary constraints contained two parts of restrictions, where LB1 is the constraint for spring phenology less than 200 days and LB2 was the constraint for autumn phenology more than 180 days (Wu et al. 2021; Xin et al. 2020). The meteorological variable constraints considered the influence of the photosynthetic rate equation, water balance equation, and temperature equation on phenology. Where $\omega 1, \ldots \omega 6$ were the weights of the six meteorological variables identified by the model. The weights of the six meteorological variables were defined with initial values ranging from 0 to 1 based on the importance results of the random forest (RF) model. Temperature and precipitation were assigned a weight of 0.6, while daylight and radiation received weights of 0.4 and 0.3, respectively. Water vapor was assigned a weight of 0.2. The weights could be adjusted when the automatic training and identification result of the model was available. The λ were the six meteorological factors used as constraints for the model inputs. The model was trained using different weighting ratios as constraints, and once the total loss reached its optimal

level, it was employed as the training model for subsequent predictions.

In the section dedicated to physical constraints, meteorological constraints occupy a strategic position. The physical constraints were derived from the weights assigned to six meteorological factors, which are determined through the training process step of the deep neural network in our model. The six meteorological variables utilized in our analysis are based on 1 km grid data. Given that vegetation phenology is primarily influenced by photosynthesis and transpiration, we chose daylight duration, vapor pressure, precipitation, temperature, and radiation as physical constraints. During the input phase of our model, each of these six meteorological variables is assigned an importance value through the training process. These importance values are subsequently used to determine the weight (ω) of each variable. The cumulative sum of these meteorological factors for each component then serves as the constraining factor for the meteorological variable section.

3.2.3. Feedback mechanism architecture

This model further utilized a sophisticated optimizer and loss function to minimize the overall error. We defined a closure method that combined the optimization to facilitate the loss function during each iteration. The closure function performs several critical tasks essential for the training of a neural network model. The optimization employed the LBFGS (Limited-memory Broyden Fletcher Goldfarb Shanno) algorithm (Lin et al. 2023; Yan et al. 2024). This optimizer algorithm was initialized with the parameters of a neural network model, with a learning rate set to 1.0. To monitor previous iterations, the maximum iteration and evaluation counts were set to 50,000. A history size of 50 was chosen to address high-dimensional problems. To adjust the optimization process and terminate further iterations, a tolerance value of 1e-5 was set for gradient convergence. Tolerance change refers to the threshold for changes in the parameters. It was set to a very small value based on the machine precision for floating-point numbers. If the change in the model parameters falls below this threshold, the optimizer assumes convergence and stops the optimization. During the optimization process, a line search function employing the strong condition was used to determine the step size along a given search direction. This line search

method helps identify an appropriate step size that effectively reduces the objective function while ensuring stability and convergence by satisfying certain conditions. Moreover, an iteration counter was initialized to keep track of the progress of the optimization process.

The loss function initialized the gradient parameters to zero in the model, preventing the accumulation of gradients from previous iterations and ensuring each iteration gradients based solely on the current loss. It is a crucial component in the training loop of neural networks, enabling the model to learn from the provided data and improve its predictive capabilities. Subsequently, the model compared the prediction value (u(pred)) with the corresponding true value (y(label)), which was computed the mean squared error (MSE) loss as the prediction error of the loss function $\mu_1 LD(\theta)$. In addition, the loss function incorporates the physical constraint part of the error, including the boundary error ($\mu_2 LD(\theta)$) and the constraint error ($\mu_3 LD(\theta)$). The total loss was obtained by summing the MSE losses, reflecting the combined error in both the predicted outputs and constraints outputs. This loss function serves as the objective that the optimizer aims to minimize. There was a loss backpropagation that calculated the gradients of the loss function with respect to the model's parameters. These gradients inform the optimizer about how to adjust the parameters to reduce the loss. Finally, the method returns the computed loss, which is then used by the optimizer to update the model's parameters in subsequent steps.

3.3. Model assessment

This model was applied to identify the phenology of four vegetation types (EV, DV, SF and SDV) in North America. The training process was executed on the PyTorch framework based on the NVIDIA RTX3070Ti. The input dataset included more than 46,000 EVI2 images derived from the MOD09Q1 spanning from 2001 to 2021. Matching labeled datasets were obtained from field observations by PhenoCam and USA-NPN. The validation dataset from PhenoCam has 815 site-year comprising a total of 56 different stations. USA-NPN has 4918 spring labeled datasets and 4214 autumn labeled data for the model. We randomly selected 70% of the dataset as labeled data

for training and the remaining 30% as test data for model testing.

The SHapley Additive exPlanations (SHAP) is a method employed to interpret the output of the model, drawing inspiration from game theory and local explanations (Antwarg et al. 2019; Parsa et al. 2020). This method allows us to estimate the impact of each individual feature on the model predictions (Antwarg et al. 2019; Parsa et al. 2020). Each feature contributes to the model output based on its marginal contribution (Slack et al. 2020). The computation of ϕi will adhere to the following algorithmic framework:

$$\phi i = \sum_{s \subseteq N\{i\}} \frac{|S|!(n - |S| - 1)!}{n!} [\vartheta(S \cup \{i\}) - \vartheta(S)] \quad (1)$$

where N represents the set of all input features and ϕi denotes the individual contribution of feature i to the model output $\vartheta(N)$, which is allocated based on their marginal contribution to each feature.

To gain a deeper understanding of the contributions of individual features, we employ feature attribution methods. In this approach, g in the algorithm serves as a linear function that represents the attribution values of the features.

$$g(Z' = \phi 0 + \sum_{i=1}^{M} {}_{\phi i Z'} \text{i}) \quad (2)$$

where M represents the number of input features, ϕi signifies the attribution value of the specific feature i. Additionally, Z' is a binary variable that takes a value of 1 when a feature is observed and 0 when it is not.

The accuracy of the vegetation phenology estimation was evaluated in comparison to that of the PhenoCam and USA-NPN stations situated across North America. Moreover, we compared the results from different models, including traditional amplitude threshold (AT) (Fischer 1994) and curvature change rate (CCR) (Zhang et al. 2003) methods, as well as artificial neural network (ANN) (Wang et al. 2019) and RF (Wang et al. 2019) models that without physical constraints. To maintain consistency with the PCNNs model, both the ANN model and RF model structures had 50 layers. Finally, an exploration was conducted to analyze the spatial heterogeneity and seasonal changes in vegetation phenology simulation outcomes across the PCNNs model.

In this study, we conducted a comprehensive assessment of the precision estimation within the different models using various evaluation metrics. These metrics included the coefficient of determination (R^2), the mean bias error (MBE), the root mean square error (RMSE), and the Willmott's index of agreement (WIA) (Willmott et al. 1985). The MBE values provide insights into the systematic bias of the model predictions, indicating whether the model tends to overestimate or underestimate the target variable. The RMSE provides a measure of the overall scatter of the model predictions compared to the actual observations, while the WIA values provide a measure of the weighted impact of the errors on the overall performance. The WIA function serves as a standardized measure that considers both the inaccuracies of model predictions and the presence of systematic biases.

3.4. Trends and relationship analysis

The analysis of vegetation phenology results in North America, spanning a period of twenty years, will be conducted using robust statistical methods. Specifically, we employ the Theil – Sen slope (Vannest et al. 2012; Wilcox 1998), a nonparametric approach that calculates the median of all possible pairwise slopes to estimate the overall trend or slope of the dataset (Burns, Klaus, and McHale 2007; Zhou et al. 2023). This method effectively quantifies the average rate of change over time, enabling us to discern whether there are increasing or decreasing trends within the study period.

Additionally, we will utilize the Mann-Kendall (Gocic and Trajkovic 2013; Yue and Wang 2002) test to further analyze and verify these trends and changes in vegetation phenology. The Mann-Kendall test is utilized to assess the statistical significance of trends within a dataset, while considering potential outliers or fluctuations. It serves to detect the existence of a monotonic increasing or decreasing trend in time series data, indicating whether there is a consistent upward or downward trend over time.

Furthermore, Pearson correlation analysis is a pivotal statistical technique for elucidating the complex relationships between vegetation phenology and various meteorological factors. In this study, we executed the correlation by the correlation function as a quantitative metric to analyze the strength of the associations between these variables.

4. Results

4.1. Spatial patterns of the prediction results

Figure 6 shows the spatial distribution of satellite-derived vegetation phenology across North America in the year of 2019. This visualization provides a detailed comparison of five distinct methods (AT, CCR, RF, ANN, and PCNNs) employed to retrieve spring and autumn vegetation phenology. The spatial patterns of SOS, EOS, and GLS exhibit a consistent variation from south to north across all five methods.

The first row indicates the spring vegetation phenology metric of SOS results using different methods, and the figure clearly depicts the gradual delay of SOS from south to north in the study area. Among these methods, spring phenology occurs at the end of
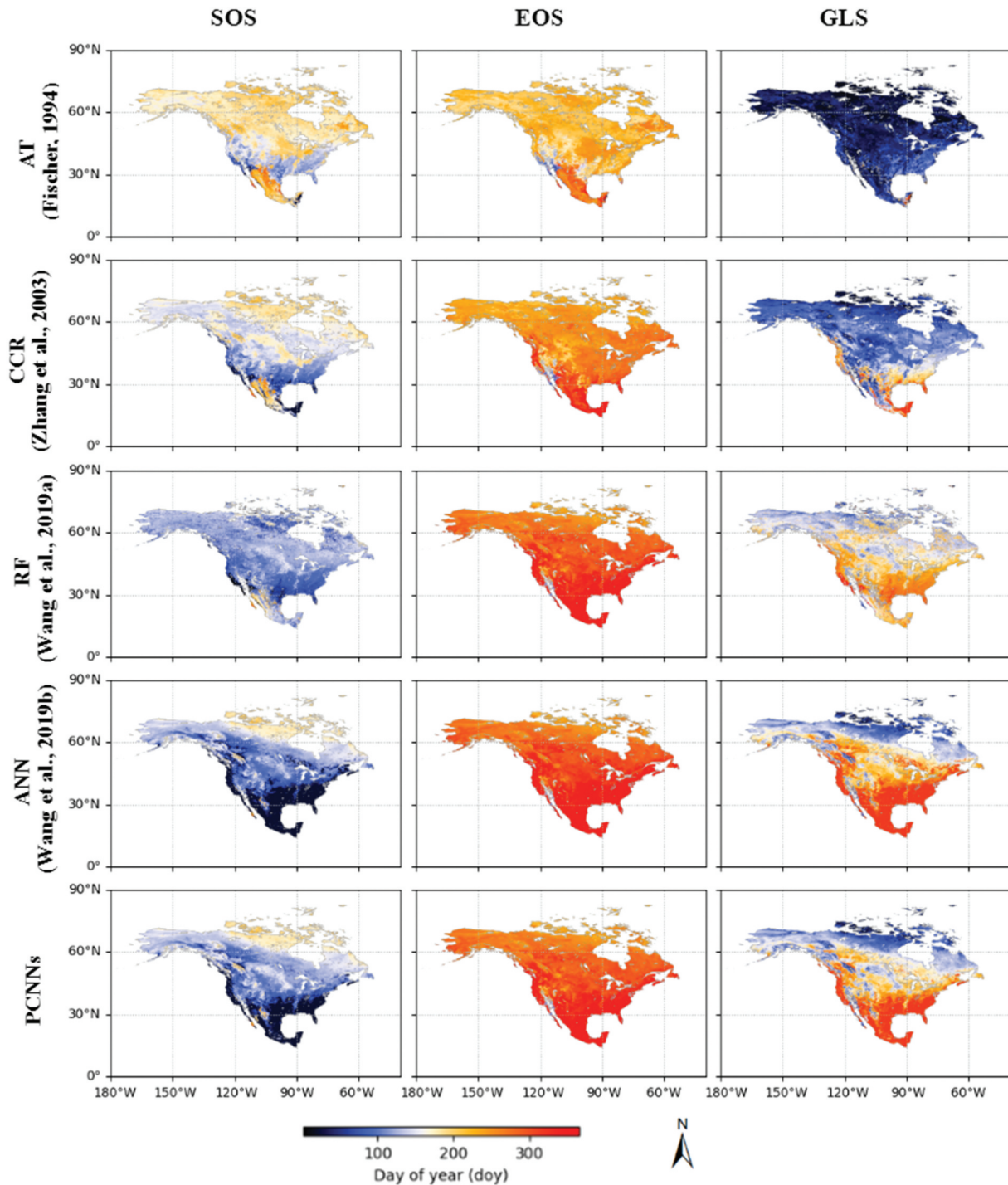

Figure 6. The vegetation phenology across North America was derived from the MODIS EVI2 time series in 2019 using five various methods, including the amplitude threshold (AT), curvature change rate (CCR), random forest (RF), artificial neural network (ANN) and PCNNs methods.

March or beginning of the April month in the south zone of blue color. There is a general observation that the SOS in the south-central region is earlier than the SOS in the northern region, especially for the results of CCR, RF, ANN and PCNNs methods. The results of the AT and CCR methods show delays in the northern part of the study area in terms of the SOS than the other methods, which shows the onset of vegetation growth ranging from DOY 190 to DOY 210. The spring phenology in the central study area exhibits advanced to DOY 70, while in the southern arid regions it is DOY 90 and in the tropical region it is DOY 190. This obvious variation suggests a strong correlation between the spring vegetation phenology and climatic conditions. At low latitudes below 30°N, the SOS is mainly concentrated in late March or early April when there are less than DOY 100 in a calendar year. At higher latitudes with more than 60°N, the SOS occurs at the end of May or beginning of June (ranging from DOY 150 to DOY 210) by AT and CCR method. This difference highlights the complexity of the spring season and the need for further research on the factors affecting the latitudinal and climatic distribution.

The EOS row in Figure 6 specifically shows the spatial distribution map of autumn phenology using five different methods across North America. The result presents that these methods obtain similar spatial patterns of autumn phenology, which illustrates the vegetation phenological metric of EOS all exceed DOY 210 in the study area. The EOS in the study area showed a gradual advancement from south to north (red to orange color), which reflected the trend along the latitudinal gradient and the effect of temperature on vegetation senescence. Specifically, the CCR and AT methods show that the EOS was significantly advanced to July (DOY 205) or August (DOY 235) in the northwestern zone of the study area. The EOS in the southwest region typically occurs between DOY 295 and DOY 320 in October or November of each year. In the tropical regions of low latitudes, the onset of autumn phenology typically occurs nearer to the months of beginning November (DOY 310) and December (DOY 350). The middle and low latitudes show a delay in EOS, which contrasts with the SOS results for the same region.

The bottom row shows the GLS results, which show a range of variations across North America. Consistent with the SOS and EOS models, the duration of the GLS shows a gradient from north to south. The southern regions demonstrate an extended period of vegetation phenology with growth cycles lasting more than 225 days such as the orange color in the GLS row, whereas the northern regions exhibit shorter growth cycles from 75 days to 115 days in the blue color of GLS row. The predicted results for RF, ANN and PCNNs show that GLS has a duration of seven or eight months which range from 195 days to the 235 days in the middle and low latitude regions, while the GLS in the northern region has a growth period of four or five months range from 105 days to 185 days in the blue color of GLS row. In the predicted results of AT and CCR methods, the growth length of vegetation phenology shows even shorter to 45 days in the northern region. This result was influenced by the correlation with latitude, as GLS has a shorter growing period from 210 days to less than 150 days along the latitude from south to north.

Figure 7 presents scatter plots comparing the field-observed and satellite-retrieved vegetation phenology for four distinct vegetation types: EV, DV, SF and SDV. The plots are based on the predictions generated by the PCNNs model. For the spring phenology predictions on the USA-NPN dataset, the model achieved an WIA value of 0.67 for EV, 0.73 for DV, 0.63 for SF and SDV. The root mean square error (RMSE) was 12.23 days for EV, 5.71 days for DV, 13.28 days for SF, and 20.53 days for SDV, demonstrating the model's precision for different vegetation types. For the EOS predictions, the model performed with an R^2 of 0.80 for EV, 0.72 for DV, 0.78 for SF, and 0.68 for SDV, showcasing a good fit between observed and predicted data. The mean absolute error (MBE) was 10.69 days for EV, 2.35 days for DV, 11.51 days for SF, and 19.71 days for SDV, highlighting the ability of our model to minimize the average magnitude of errors in predicting the timing of EOS. The closeness of the points to the diagonal line indicates the accuracy of the model's predictions, with points closer to the line suggesting better agreement between the observed and predicted values. The figure provides valuable insights into the performance of the PCNNs model in capturing the phenological patterns of different vegetation types, highlighting its potential for applications in monitoring and predicting vegetation dynamics.
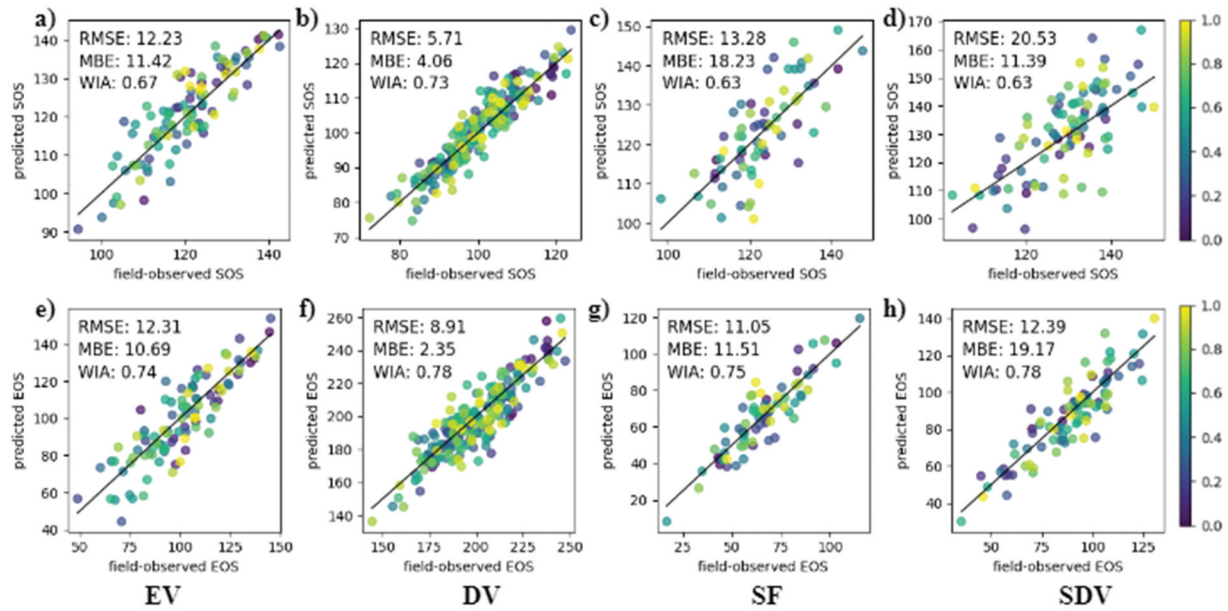
Figure 7. Scatter plots between the field-observed and satellite-retrieved vegetation phenology of four vegetation types (EV, DV, SF, and SDV) based on the PCNNs model. The first row shows the validation results of SOS on the USA-NPN dataset, and the bottom row shows the validation results of EOS on the USA-NPN dataset. Note: EV: evergreen vegetation; DV: deciduous vegetation; SF: shrub forests; SDV: stressed deciduous vegetation.

4.2. Phenology of four distinct vegetation types

We conducted an evaluation of the performance of five distinct models – AT, CCR, RF, ANN and PCNNs – across four specific vegetation types (EV, DV, SF, and SDV). This assessment incorporated various evaluation metrics (RMSE, MBE, and WIA) to rigorously determine the effectiveness of each model. The Taylor diagram in Figure 8 illustrates the performance of five vegetation phenology extraction methods using three evaluation metrics in comparison to the available data for all vegetation types. The results of the five methods varied across different vegetation types. Among the four vegetation types evaluated using PhenoCam data, the DV yielded more accurate vegetation phenology predictions compared to the other vegetation types. For SOS predictions (Figure 8a), DV exhibits better and more stable results with a standard deviation of 3 days in the PCNNs, while the prediction for the SF shows the least accuracy among the four types with RMSD errors of 23 days by AT approach. For EOS predictions (Figure 8b), the EV and DV types demonstrate better predictions of vegetation phenology compared to the other vegetation types, with standard deviations with 5 days and 2 days, respectively. The SDV shows relatively larger prediction error with greater standard deviations (28

days) and RMSDs (23 days), indicating a larger dispersion of prediction results for this vegetation type. The deep learning-based methods of ANN and PCNNs (show the solid squares and diamond shape symbols, respectively) performed similarly in EV with the error of 11 days, while RF model performed inferiorly to the other methods. For the SDV type, the AT and CCR methods had a clear advantage over the machine learning method. Across vegetation types, the machine learning methods had almost identical correlations that were higher at about 0.7, while the CCR method had a lower correlation of about 0.5. Overall, the machine learning-based approach produced better results than the other two methods (AT and CCR).

In addition to comparing the differences in the spatial distributions of vegetation phenology extracted using the different approaches, we also conducted a trend analysis of average phenology along the latitudinal for four vegetation types. The Figure 9(a–c) shows the average vegetation phenology trends along the latitude, and the Figure 9(d–f) shows the results of average vegetation phenology for the four vegetation types. Among the four vegetation types in Figure 7(a), the growth length of SDVs varies very little throughout the latitudinal period with the GLS
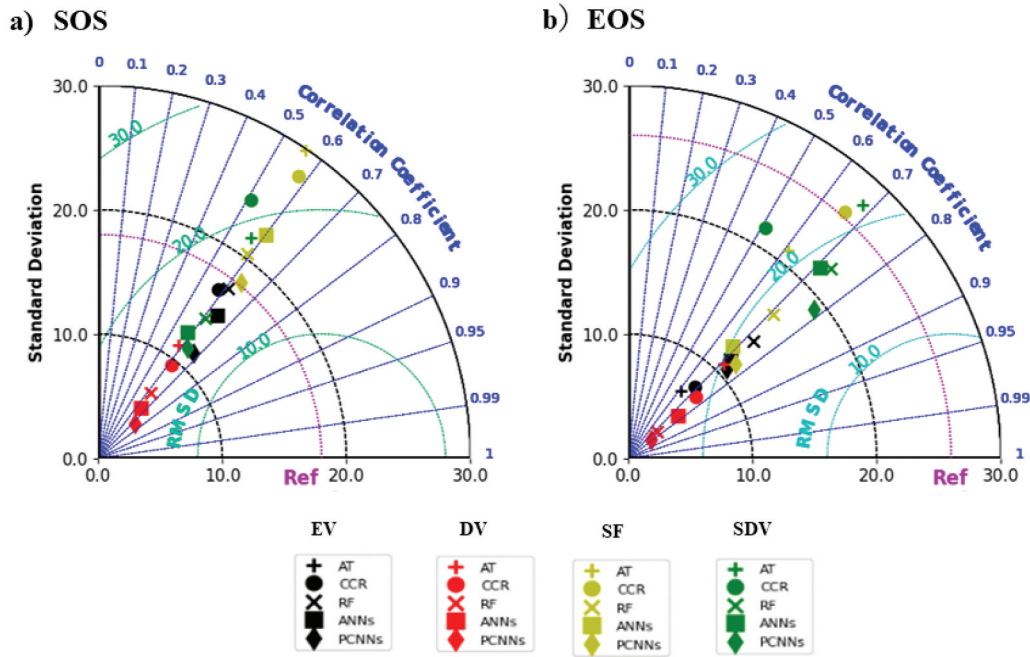
Figure 8. The Taylor diagram comparing five satellite-derived phenology retrieval methods for a) start of season (SOS) and b) end of season (EOS) in four vegetation types. The blue color in the figure represents correlation coefficient, the black color represents standard deviation, and the color of cyan represents RMSD. The five different methods are represented by different shape symbols. Note: EV: evergreen vegetation; DV: deciduous vegetation; SF: mixed forests; SDV: stressed deciduous vegetation.

having a duration of 152 days. In higher latitudes (>60°N), the onset of spring phenology becomes later with increasing latitude. At low and middle latitudes (<60°N), the autumn phenology of SDV occurs later in DOY 285 within a calendar year. At the latitude of 40°N, the SOS of SF vegetation shows advanced to DOY 120 and the EOS is delayed to DOY 290, resulting in a decrease in the growing period with 170 days of SF at mid-latitudes (Figure 8c). According to Figure 9(d–f), the stability of vegetation phenology start growth and end growth shows higher in DV and SF, and the variation of EV and SDV is larger than that in SF. Specifically, DV shows the earliest spring phenology, while SDV had the latest SOS. In terms of EOS, DV had the latest dormancy period reflecting the longer growth season than the other vegetation types. The latitudinal trend of SOS shows consistent in the DV with approximately DOY 90. In the middle to high latitude such as the localized areas between 40°N and near to 80°N, the SOS of DV advanced to DOY 95, and the EOS of DV shows no change with DOY 315 at the same

latitude, resulting in an increase DV growth season of 270 days. It shows that the advancement of spring phenology is the main reason for the extended growth period of DV.

4.3. Comparison of temporal trends in vegetation phenology over 20 years

We produced temporal trend maps of the annual average SOS, EOS, and GLS obtained through the application of the PCNNs methods across North America from 2000 to 2020. The colors in Figure 10(a–c) indicate the trends in vegetation phenology over the 20-year period, where red represents an increase trend and green represents a delay. Negative values signify a decreasing trend over the study period, whereas positive values denote an increasing trend. For the SOS, the Theil-Slope trend shows a positive trend in the central part of the study region. Conversely, the northeastern region exhibited a negative trend in the SOS over the study period. For the EOS, it becomes evident that the northeastern area exhibited
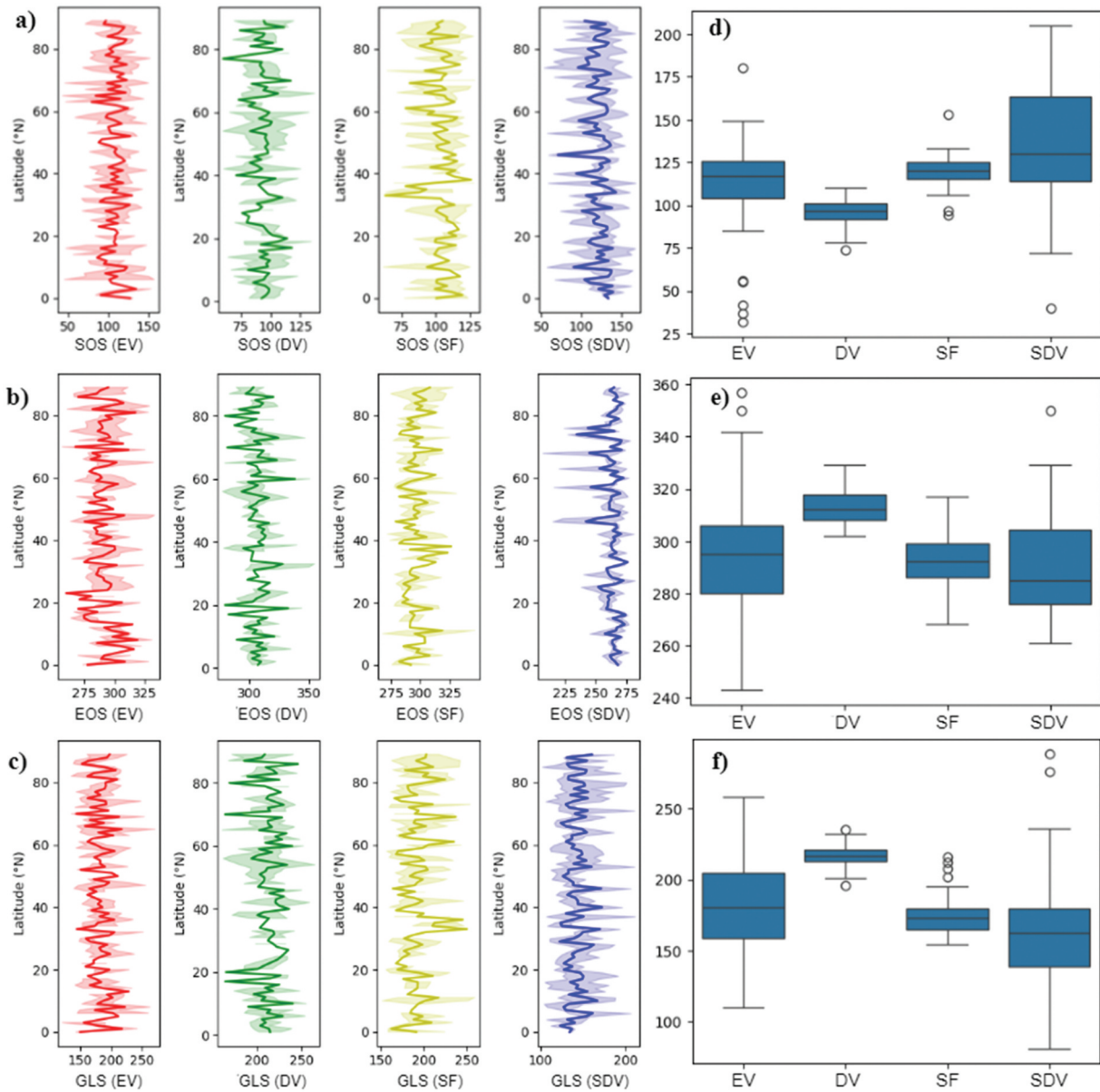
Figure 9. The vegetation phenology variation along the latitude across North America (a-c). The box plot diagrams (d-f) show the vegetation phenology of the four vegetation types from 2001 to 2021. The solid line of latitude diagram represents the vegetation phenology trends for four different vegetation types along different latitudes. The inner shaded area in the panel is the 95% confidence interval. a) and d) represent the SOS, b) and e) represent the EOS, c) and f) represent the GLS, respectively. Note: EV: evergreen vegetation; DV: deciduous vegetation; SF: mixed forests; SDV: stressed deciduous vegetation.

a more prominent upward trend than the north-western region.

Figure 10(d–f) shows the vegetation phenology change trends of the four vegetation types from 2001 to 2021. The trends of the four vegetation types were examined by Mann-Kendall, the p-values were all less than 0.05 and showed a significant result. The four vegetation types exhibited an increase in GLS over the study period. SDV shows the largest increasing trend in GLS with a value of 0.43 day/year. SF and EV display

similar increases of approximately 0.25 day/year, while DV shows the smallest increase in GLS at 0.08 day/year. Regarding the SOS for the vegetation, DV shows the smallest increase in delay during the growth time, with a trend of 0.11 day/year. EV and SF exhibit an advance trend during the growth time, with values of −0.51day/year and −0.45 day/year, respectively. All four vegetation types of EOS experience a postponement during the growth period of 20 years. EV shows the maximum rate of change with
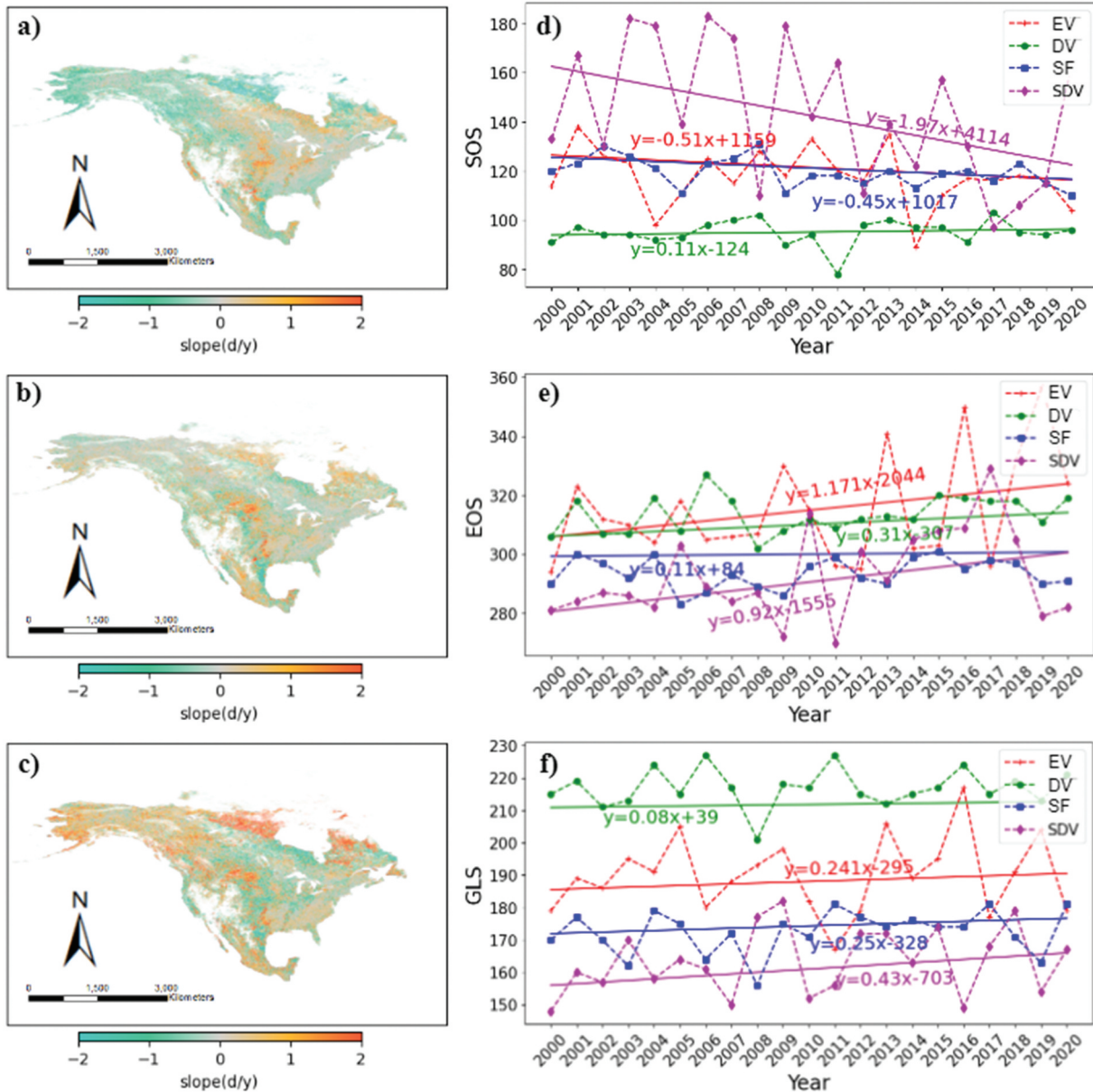
Figure 10. Temporal trend in the annual average values of vegetation phenology in North America from 2001 to 2021. a) to c) are the overall trends in phenology for all vegetation types. d) to f) are the annual phenological trends for the four categories of vegetation types. EV: evergreen vegetation; DV: deciduous vegetation; SF: mixed forests; SDV: stressed deciduous vegetation.

a 1.17 day/year, while SDV had the smallest deferral rate of 0.05 day/year. DV and SF display relatively smaller increases in the EOS, with values of 0.31 day/ year and 0.11 day/year, respectively. The greatest change in vegetation type was observed in the SDV during the study period. During the onset growth period, vegetation growth time shows progress with a trend of −1.97 day/year over the 20-year period. The vegetation phenology growth period is delayed during the EOS phase, with an increase of 0.02 day/year.

The overall duration of the growth period increased by 0.43 day/year during the period of 20 years.

4.4. Relationships between meteorological variables and vegetation phenology

We conducted a comprehensive analysis of the correlations between six meteorological variables and the mean vegetation phenology from 2001 to 2021. The
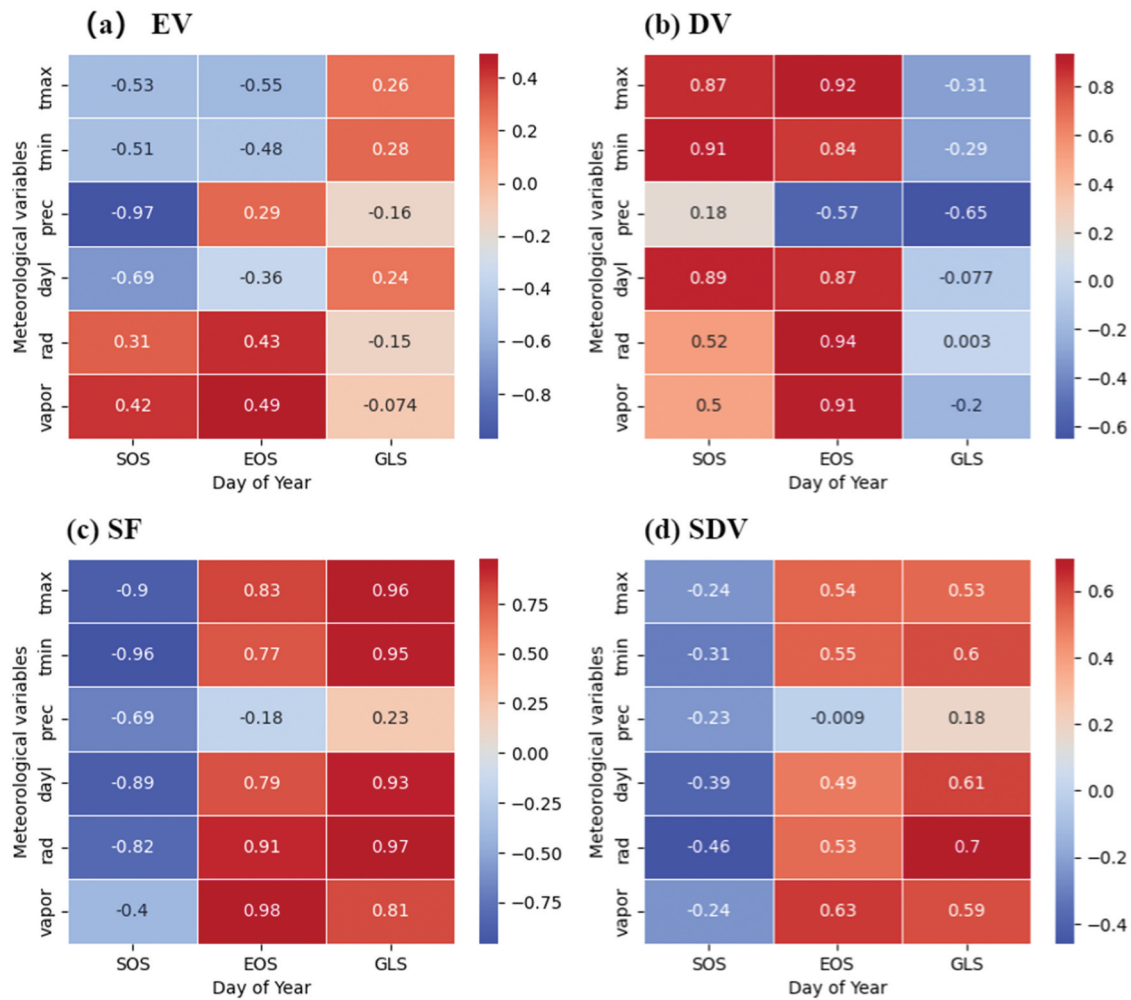
Figure 11. The heatmap of correlations between phenology and meteorological variables for different vegetation types from 2001 to 2021. (a) evergreen vegetation (EV), (b) deciduous vegetation (DV), (c) shrub forests (SF), and (d) stressed deciduous vegetation (SDV).

results presented in Figure 11 offer a comprehensive analysis of the relationships between the six meteorological variables and vegetation phenology for the different vegetation types. The heatmap illustrates the interactions of EV, DV, SF, and SDV with vegetation phenology for 20 years. The heatmap utilizes colors to effectively emphasize the relationships, with red indicating a positive correlation and blue denoting a negative correlation. The result shows that while there are discernible patterns in the relationships between vegetation phenology and meteorological variables across different vegetation types, the strength and direction of these correlations vary significantly. More specifically, the SOS was negatively correlated with each of the meteorological variables for SF and SDV and positively correlated with each of the meteorological variables for SOS and DV. The air temperature and day length of DV had strong positive correlations with the SOS of 0.87 and 0.89, respectively. EV and SF had strong negative correlations with precipitation and daylength of −0.96 and −0.89, respectively. EOS was negatively correlated with precipitation for DV (−0.57), SF (−0.18), and SDV (−0.009), and EOS was positively correlated with most other variables. Compared to other meteorological variables, vapor had a strong positive correlation of more than 0.49 with the EOS in each vegetation type. Precipitation had a strong negative correlation with the EOS except for EV (0.29). The analysis revealed a highly significant correlation of GLS, exhibiting a positive association with SF and SDV, whereas it demonstrated a negative correlation with all meteorological variables pertaining to DV. Specifically, within the SF vegetation types, the correlation coefficient exceeded 0.93 for all metrics, with the exception of precipitation, which exhibited a relatively weak

correlation of 0.23 with GLS. On the other hand, the positive correlation between GLS and individual meteorological variables for the SDV was not particularly strong but was consistently positive. Similarly, the negative correlation between meteorological variables and GLS for DV was also near nonsignificant, with all correlation coefficients falling below 0.31.

5. Discussion

5.1. Physical constraints in the ML model

The PCNNs model outperforms other approaches in predicting vegetation phenology, as evidenced by the results presented in Tables C1 and C2. This indicates that the model embedded with physical constraints can identify vegetation phenology better than other methods without physical constraints. The PCNNs model incorporates three physical constraint components for vegetation phenology, as depicted in Figure 5. The first component is labeled constraints, which restricts the models that can be trained well based on labeled data (Melaas, Friedl, and Zhu 2013; Wang et al. 2019). The second component is boundary constraints, which restrict the SOS and EOS results based on the characteristics of spring and autumn vegetation phenology (Buttò et al. 2023; Kowalski et al. 2020). The meteorological constraint part is the most crucial part for this model, which considers the physical mechanisms of photosynthesis and transpiration processes in vegetation growth. The six meteorological variables in the PCNNs are essential in adjusting each meteorological factor for this model. These components suggest that the incorporation of physical constraints in the model takes into account the complex environmental factors during vegetation growth, making it applicable to more complex environmental scenarios. The ML methods (RF and ANN) used in this study do not employ physical constraints and identify vegetation features only from the EVI2 time series, which do not consider the complex physical mechanisms. Traditional rule-based methods (AT and RCC) underestimate or overestimate the duration of the growing season due to differences in algorithms and sensitivity to various environmental factors (Purdy et al. 2023; Wang et al. 2023; Xie et al. 2023). Previous studies mainly considered the temperature or precipitation in the rule-based method, but all of them only accounted for one or two variables and assumed linear relationships (Shen et al. 2011; Tian et al. 2024). Given the complex physical mechanisms of vegetation growth, these rule-based methods need to consider more meteorological factors and more complicated physical processes.

More complex vegetation types require stricter physical constraints to accurately predict the vegetation growth patterns. The box plot analysis of the DV and SF vegetation types exhibits greater stability compared to the EV and SDV vegetation types (Figure 7). DV had longer growth length than the other vegetation types, indicating that the DV vegetation type has a more favorable growing environment (Kowalski et al. 2020; Melaas, Friedl, and Zhu 2013). This can be attributed to the biological characteristics of the DV vegetation, such as thicker roots and trunks, larger leaves, and better adaptability to diverse climatic conditions (Hufkens et al. 2012; Yang et al. 2021). Additionally, EV and SDV vegetation types have narrower and thinner leaves that are less susceptible to photosynthesis and transpiration (Kowalski et al. 2020; Peng et al. 2021; Silveira et al. 2024). In this context, the PCNNs model effectively integrates the physical mechanisms of vegetation growth, incorporating meteorological factors related to photosynthesis and transpiration. By embedding these physical constraints within the model, it surpasses other methods in terms of accurately predicting vegetation phenology.

The integration of physical constraints within the ML model also has a wide range of applications in engineering and biology fields. Physical constraints ensure that a system or individual follows a predetermined trajectory and speed, enabling precise control and manipulation (Lin et al. 2023; Yan et al. 2024; Zang et al. 2021). In this study, the input datasets for the model are EVI2 time series rather than imagery, which increases the complexity and time cost for the whole model process. Moreover, variations in model structures and parameters used in current satellite data smoothing methods can lead to inconsistent results (Wang, Zhang, and Rodman 2021). While embedding physical constraints enhances the reliability of the PCNNs model, it is crucial to strike a balance between incorporating these constraints and maintaining model efficiency. To comprehensively evaluate model performance,

additional factors such as stability, computational complexity, and data adaptability should be considered. Future research should aim to achieve a harmonious balance between model efficiency and the simulation of complex physical processes. This can be accomplished by developing efficient and robust algorithms that can effectively handle intricate physical constraints while preserving model performance. Moreover, there is a need to develop more reliable and sustainable vegetation phenology prediction models that cater to the diverse demands of a wide array of applications.

5.2. Selection of meteorological variables in vegetation phenology

In this paper, we considered the photosynthesis and transpiration processes that are closely related to vegetation growth. The employed model identifies meteorological factors associated with vegetation growth and assigns different weights to each factor. By selecting the key meteorological factors of these two physical mechanisms of the vegetation growth process, the model generates output results that enhance the accuracy of vegetation phenology predictions. In addition, it is important to note that the growth of vegetation types is influenced by a multiple of factors, including respiration, carbon exchange and other physical mechanism effects (He et al. 2024; Migliavacca et al. 2015). Meteorological variables such as carbon dioxide and oxygen, which are intricately linked to respiration, can serve as additional physical constraints on vegetation phenology (Curiel Yuste et al. 2004; Keenan et al. 2014). In future studies, it would be valuable to incorporate meteorological factors associated with respiration such as carbon dioxide, into the PCNNs model to further explore their impact on vegetation dynamics.

The dominant meteorological factors affecting vegetation phenology vary across different regions. The study area spans a wide latitude and diverse climate zones in the North Hemisphere, as shown in Figure 6. The southern part boasts a subtropical monsoon climate characterized by higher temperatures and rainfall compared to other regions. This climate fosters the growth of extensive subtropical forests in this region. The Rocky Mountain in the southwestern part has a complex topography that influences vegetation growth through factors like altitude, slope

orientation, and slope gradient, consequently impacting vegetation phenology. There were various shifting patterns of the same vegetation type along latitude in Figure 7, indicating that changes in vegetation phenology are also affected by latitude. The reason for this is that meteorological factors, such as temperature, radiation and daylight, vary significantly at different latitudes (Gu et al. 2023; Wang et al. 2022; Zhang et al. 2004). These findings demonstrate the importance of meteorological variables in distinct climatic zones when influencing vegetation phenology within the study region. Therefore, future research could explore the dominant meteorological influences on vegetation phenology in diverse climate regions, as well as explore how the phenology of different vegetation types varies along latitude gradients.

Previous traditional rule-based methods generally focused on the effects of temperature or precipitation on vegetation phenology separately (de Beurs and Henebry 2005; Guo et al. 2021; Shen et al. 2011), without exploring the impact of multiple meteorological variables comprehensively. Although this study considers six meteorological factors, each factor was not extensively examined in more detail for different regions. The different vegetation types may be affected by different meteorological factors, further work could delve into the vegetation phenology dynamics of two or more meteorological variables for a wider range of vegetation types. The quality and properties of the soil, such as fertility, pH, and moisture content, can influence the vegetation growth and phenology (Caldas et al. 2018; Cui et al. 2022; Francioli et al. 2018). Different vegetation types have different soil preferences, and favorable soil conditions can promote earlier and more vigorous growth (Francioli et al. 2018; Luo et al. 2021). Therefore, the influencing factors about soil conditions could also be considered in future studies. Overall, multiple meteorological variables including different vegetation types or different regions should be considered in the future to accurately reveal the physical mechanisms and patterns of vegetation phenology dynamics.

5.3. Strengths and limitations

This study integrated physical constraints within machine learning frameworks to retrieve the variations

in vegetation phenology. Previous predictions of vegetation phenology have mainly relied on time series (Peng et al. 2017; Zhang et al. 2022; Zhang et al. 2003) or deep learning methods (Cao et al. 2021; Wu et al. 2014; Wu et al. 2021; Zhou et al. 2021). The traditional time series approach to retrieve the vegetation phenology depends on the availability of a complete time series. However, deep learning methods often overlook the intricate physical processes underlying vegetation phenology. The main contributions of this study are concluded as follows: First, this paper introduces an artificial intelligence-based approach for predicting vegetation phenology that uniquely incorporates physical mechanisms into the prediction process. Given the intricate nature of these mechanisms, prior deep learning methods have overlooked the specific physical processes involved in vegetation prediction, which is addressed in this study. This integration of physical mechanisms significantly enhances the prediction accuracy of machine learning models. Second, this study examined the intricate relationships between multiple climate factors and vegetation phenology, elucidating the impacts of these factors. In contrast to existing research that has focused primarily on the influence of one or two meteorological factors, this study comprehensively considered six major vegetation phenology factors, thereby providing a deeper understanding of the interplay between climate and vegetation phenology.

Despite the progress made in this research, uncertainties persist in the estimation of vegetation phenology. These uncertainties may arise from various sources, such as errors in remote sensing data, limitations in the model itself, or inadequate representation of physical processes. Moreover, there are significant differences in the model structure and parameters used in the current smoothing methods for satellite data, which may lead to inconsistencies in the results (Wang, Zhang, and Rodman 2021). The model considered the effects of meteorological variables on photosynthesis and transpiration. However, it does not account for meteorological variables of other biochemical processes affecting the growth of vegetation phenology, such as respiration and carbon exchange. The meteorological factors of carbon dioxide and oxygen on vegetation respiration remain unconsidered. This study focuses on a pixel scale rather than a site level, it could compare the predictions at a diverse scale for further study (Wang et al. 2017). Moreover, it is crucial to consider the influence of

urbanization and human activities, as well as climate conditions on plant phenology (Ren et al. 2018; Vitasse et al. 2022; Zhou et al. 2016). Future research should aim to quantify these uncertainties and identify potential ways to mitigate them. For example, the use of advanced remote sensing techniques or the integration of auxiliary datasets could help improve the accuracy of vegetation phenology estimates. Satellite datasets with higher spatial and temporal resolutions need to be employed for extracting vegetation phenology metrics. Additionally, the development of more sophisticated vegetation phenology models that can better represent complex physical processes and interactions could further enhance the reliability of assimilation results. This integrated approach will improve the accuracy and reliability of vegetation phenology assessments and provide valuable insights into the complex interactions between vegetation, climate and anthropogenic factors. By addressing these uncertainties and incorporating additional data and models, future research can further improve the accuracy and reliability of spatial assimilation schemes for vegetation phenology prediction.

6. Conclusions

This study developed a novel model of PCNNs specifically designed to identify vegetation phenology in North America. The model involves six major meteorological variables that influence the vegetation phenology process and train the PCNNs model based on their different weighting of each factor. Embedding physical constraints in ML approaches offers several significant benefits: 1) Enhanced prediction accuracy: By leveraging physical knowledge, ML models are better equipped to capture the inherent behavior of phenological processes, leading to more accurate and reliable predictions. 2) Novel insights: The integration of physical constraints opens up a new avenue for understanding the intricate relationships between phenology and environmental factors, potentially leading to the discovery of new scientific insights. 3) Improved model development: Embedding physical constraints can facilitate the development of more robust and reliable phenology models by guiding them toward physically plausible solutions.

The results of this study demonstrate that the PCNNs model delivers more accurate predictions compared to conventional models and previous approaches that are

not embedded in physical mechanisms across North America. Over the span of 20 years, all four vegetation types exhibited an extension for the growth length. The maximum change in growth trend for the SDV vegetation types was 0.43 day/year. Both EV and DV vegetation types had growth rates of approximately 0.25 day/year. The DV illustrates the highest prediction accuracy among the four models evaluated by PhenoCam and USA-NPN dataset. In terms of meteorological factor correlations, the analysis revealed that meteorological variables exerted a more profound influence on the EOS compared to the SOS. This study exemplifies the ability to extract knowledge from a limited labeling dataset for establishing the intricate relationship between vegetation phenology and related environmental factors.

The findings of this study hold significant implications for enhancing our ability to predict vegetation phenology in different climatic zones under complex climatic conditions. By considering the interactions between the physical processes of vegetation phenology and meteorological variables, we can gain a deeper understanding of ecosystem functioning and deepening our comprehension of ecosystem dynamics. Incorporating physical constraints into machine learning models has the potential to improve the accuracy and reliability of vegetation phenology predictions, ultimately contributing to more effective land management strategies, climate change mitigation, and ecological conservation efforts.

Acknowledgments

Disclosure statement

No potential conflict of interest was reported by the author(s).

Funding

Author contributions statement

Mengying CAO: Conceptualization, Data pre-processing, Methodology, Analysis, Software, Validation, Visualization, Writing – original draft. Qihao Weng: Conceptualization, Funding acquisition, Methodology, Project administration, Resources, Supervision, Validation, Writing – review and editing.

Data availability statement

The coding scripts in this article can be accessed at https://github.com/caomy7/PCNNs.

ORCID

Qihao Weng http://orcid.org/0000-0002-2498-0934

References

Antwarg, L., R. M. Miller, B. Shapira, and L. Rokach. 2019. "Explaining Anomalies Detected by Autoencoders Using SHAP." *ArXiv Prepr*: ArXiv190302407. https://doi.org/10.1016/j.eswa.2021.115736.

Bolton, D. K., and M. A. Friedl. 2013. "Forecasting Crop Yield Using Remotely Sensed Vegetation Indices and Crop Phenology Metrics." *Agricultural and Forest Meteorology* 173:74–84. https://doi.org/10.1016/j.agrformet.2013.01.007.

Burns, D. A., J. Klaus, and M. R. McHale. 2007. "Recent Climate Trends and Implications for Water Resources in the Catskill Mountain Region, New York, USA." *Journal of Hydrology* 336 (1–2): 155–170. https://doi.org/10.1016/j.jhydrol.2006.12.019.

Buttò, V., S. Khare, P. Jain, G. De Lima Santos, and S. Rossi. 2023. "Spatial Patterns and Climatic Drivers of Leaf Spring Phenology of Maple in Eastern North America." *Science of the Total Environment* 857:159064. https://doi.org/10.1016/j.scitotenv.2022.159064.

Caldas, A., T. Pissara, R. Costa, F. Neto, M. Zanata, R. Parahyba, L. Sanches Fernandes, and F. Pacheco. 2018. "Flood Vulnerability, Environmental Land Use Conflicts, and Conservation of Soil and Water: A Study in the Batatais SP Municipality, Brazil." *Water* 10 (10): 1357. https://doi.org/10.3390/w10101357.

Cao, M., Y. Sun, X. Jiang, Z. Li, and Q. Xin. 2021. "Identifying Leaf Phenology of Deciduous Broadleaf Forests from PhenoCam Images Using a Convolutional Neural Network Regression Method." *Remote Sensing* 13 (12): 2331. https://doi.org/10.3390/rs13122331.

Caparros-Santiago, J. A., V. Rodriguez-Galiano, and J. Dash. 2021. "Land Surface Phenology as Indicator of Global Terrestrial Ecosystem Dynamics: A Systematic Review." *Isprs Journal of Photogrammetry & Remote Sensing* 171:330–347. https://doi.org/10.1016/j.isprsjprs.2020.11.019.

Cheng, Y., A. Vrieling, F. Fava, M. Meroni, M. Marshall, and S. Gachoki. 2020. "Phenology of Short Vegetation Cycles in

a Kenyan Rangeland from PlanetScope and Sentinel-2. Remote Sens." *Remote Sensing of Environment* 248:112004. https://doi.org/10.1016/j.rse.2020.112004.

Cui, D., S. Liang, and D. Wang. 2021. "Observed and Projected Changes in Global Climate Zones Based on Köppen Climate Classification." *WIREs Climate Change* 12 (3): e701. https://doi.org/10.1002/wcc.701.

Cui, X., G. Xu, X. He, and D. Luo. 2022. "Influences of Seasonal Soil Moisture and Temperature on Vegetation Phenology in the Qilian Mountains." *Remote Sensing* 14 (15): 3645. https://doi.org/10.3390/rs14153645.

Cuomo, S., V. S. Di Cola, F. Giampaolo, G. Rozza, M. Raissi, and F. Piccialli. 2022. "Scientific Machine Learning Through Physics–Informed Neural Networks: Where We are and What's Next." *Journal of Scientific Computing* 92 (3): 88. https://doi.org/10.1007/s10915-022-01939-z.

Curiel Yuste, J., I. Janssens, A. Carrara, and R. Ceulemans. 2004. "Annual Q10 of Soil Respiration Reflects Plant Phenological Patterns as Well as Temperature Sensitivity." *Global Change Biology* 10 (2): 161–169. https://doi.org/10.1111/j.1529-8817.2003.00727.x.

de Beurs, K. M., and G. M. Henebry. 2005. "Land Surface Phenology and Temperature Variation in the International Geosphere–Biosphere Program High-Latitude Transects." *Global Change Biology* 11 (5): 779–790. https://doi.org/10.1111/j.1365-2486.2005.00949.x.

De Beurs, K. M., and G. M. Henebry. 2010. *Spatio-Temporal Statistical Methods for Modelling Land Surface Phenology*. Springer Dordr. https://doi.org/10.1007/978-90-481-3335-2_9.

Elmendorf, S. C., K. D. Jones, B. I. Cook, J. M. Diez, C. A. Enquist, R. A. Hufft, M. O. Jones, et al. 2016. "The Plant Phenology Monitoring Design for the National Ecological Observatory Network." *Ecosphere* 7 (4): e01303. https://doi.org/10.1002/ecs2.1303.

Fang, H., F. Baret, S. Plummer, and G. Schaepman-Strub. 2019. "An Overview of Global Leaf Area Index (LAI): Methods, Products, Validation, and Applications." *Reviews of Geophysics* 57 (3): 739–799. https://doi.org/10.1029/2018RG000608.

Fischer, A. 1994. "A Model for the Seasonal Variations of Vegetation Indices in Coarse Resolution Data and Its Inversion to Extract Crop Parameters." *Remote Sensing of Environment* 48 (2): 220–230. https://doi.org/10.1016/0034-4257(94)90143-0.

Francioli, D., E. Schulz, F. Buscot, and T. Reitz. 2018. "Dynamics of Soil Bacterial Communities Over a Vegetation Season Relate to Both Soil Nutrient Status and Plant Growth Phenology." *Microbial Ecology* 75 (1): 216–227. https://doi.org/10.1007/s00248-017-1012-0.

Gao, F., and X. Zhang. 2021. "Mapping Crop Phenology in Near Real-Time Using Satellite Remote Sensing: Challenges and Opportunities." *Journal of Remote Sensing* 2021, 2021/8379391. https://doi.org/10.34133/2021/8379391.

Gao, X., I. R. McGregor, J. M. Gray, M. A. Friedl, and M. Moon. 2023. "Observations of Satellite Land Surface Phenology Indicate That Maximum Leaf Greenness is More Associated with Global Vegetation Productivity Than Growing Season Length." *Global Biogeochemical Cycles* 37 (3): e2022GB007462. https://doi.org/10.1029/2022GB007462.

Gocic, M., and S. Trajkovic. 2013. "Analysis of Changes in Meteorological Variables Using Mann-Kendall and Sen's Slope Estimator Statistical Tests in Serbia." *Global and Planetary Change* 100:172–182. https://doi.org/10.1016/j.gloplacha.2012.10.014.

Gu, Y., Y. Zhao, Z. Guo, L. Meng, K. Zhang, J. Wang, C. K. F. Lee, et al. 2023. "The Underappreciated Importance of Solar Radiation in Constraining Spring Phenology of Temperate Ecosystems in the Northern and Eastern United States." *Remote Sensing of Environment* 294:113617. https://doi.org/10.1016/j.rse.2023.113617.

Guo, Y., Y. Fu, F. Hao, X. Zhang, W. Wu, X. Jin, C. Robin Bryant, and J. Senthilnath. 2021. "Integrated Phenology and Climate in Rice Yields Prediction Using Machine Learning Methods." *Ecological Indicators* 120:106935. https://doi.org/10.1016/j.ecolind.2020.106935.

He, Y., B. Bond-Lamberty, A. N. Myers-Pigg, M. E. Newcomer, J. Ladau, J. R. Holmquist, J. B. Brown, and N. Falco. 2024. "Effects of Spatial Variability in Vegetation Phenology, Climate, Landcover, Biodiversity, Topography, and Soil Property on Soil Respiration Across a Coastal Ecosystem." *Heliyon Elsevier* 10 (9): E30470. https://doi.org/10.1016/j.heliyon.2024.e30470.

Helman, D. 2018. "Land Surface Phenology: What Do We Really 'See' from Space?" *Science of the Total Environment* 618:665–673. https://doi.org/10.1016/j.scitotenv.2017.07.237.

Hufkens, K., M. Friedl, O. Sonnentag, B. H. Braswell, T. Milliman, and A. D. Richardson. 2012. "Linking Near-Surface and Satellite Remote Sensing Measurements of Deciduous Broadleaf Forest Phenology." *Remote Sensing of Environment* 117:307–321. https://doi.org/10.1016/j.rse.2011.10.006.

Jiang, Z., A. Huete, K. Didan, and T. Miura. 2008. "Development of a Two-Band Enhanced Vegetation Index without a Blue Band." *Remote Sensing of Environment* 112 (10): 3833–3845. https://doi.org/10.1016/j.rse.2008.06.006.

Keenan, T. F., J. Gray, M. A. Friedl, M. Toomey, G. Bohrer, D. Y. Hollinger, J. W. Munger, et al. 2014. "Net Carbon Uptake Has Increased Through Warming-Induced Changes in Temperate Forest Phenology." *Nature Climate Change* 4 (7): 598–604. https://doi.org/10.1038/nclimate2253.

Klosterman, S. T., K. Hufkens, J. M. Gray, E. Melaas, O. Sonnentag, I. Lavine, L. Mitchell, R. Norman, M. A. Friedl, and A. D. Richardson. 2014. "Evaluating Remote Sensing of Deciduous Forest Phenology at Multiple Spatial Scales Using PhenoCam Imagery." *Biogeosciences* 11 (16): 4305–4320. https://doi.org/10.5194/bg-11-4305-2014.

Kowalski, K., C. Senf, P. Hostert, and D. Pflugmacher. 2020. "Characterizing Spring Phenology of Temperate Broadleaf Forests Using Landsat and Sentinel-2 Time Series." *International Journal of Applied Earth Observation and Geoinformation* 92:102172. https://doi.org/10.1016/j.jag.2020.102172.

Li, X. et al. 2023. "Comparing Phenocam Color Indices with Phenological Observations of Black Spruce in the Boreal Forest." *Ecological Informatics* 76: 102149. https://doi.org/10.1016/j.ecoinf.2023.102149.

Li, Y., G. Zhao, D. Shah, M. Zhao, S. Sarkar, S. Devadiga, B. Zhao, S. Zhang, and H. Gao. 2021. "Nasa's Modis/Viirs Global Water Reservoir Product Suite from Moderate Resolution Remote Sensing Data." *Remote Sensing* 13 (4): 565. https://doi.org/10.3390/rs13040565.

Li, Z., Q. Weng, Y. Zhou, P. Dou, and X. Ding. 2024. "Learning Spectral-Indices-Fused Deep Models for Time-Series Land Use and Land Cover Mapping in Cloud-Prone Areas: The Case of Pearl River Delta." *Remote Sensing of Environment* 308:114190. https://doi.org/10.1016/j.rse.2024.114190.

Liang, L., M. D. Schwartz, and S. Fei. 2011. "Validating Satellite Phenology Through Intensive Ground Observation and Landscape Scaling in a Mixed Seasonal Forest." *Remote Sensing of Environment* 115 (1): 143–157. https://doi.org/10.1016/j.rse.2010.08.013.

Lin, Z., S. Zhang, Z. Zhang, X. Yu, and Y. Gao. 2023. "The Rossby Normal Mode as a Physical Linkage in a Machine Learning Forecast Model for the SST and SSH of South China Sea Deep Basin." *Journal of Geophysical Research Oceans* 128 (9): e2023JC019851. https://doi.org/10.1029/2023JC019851.

Lohmann, U., R. Sausen, L. Bengtsson, U. Cubasch, J. Perlwitz, and E. Roeckner. 1993. "The Köppen Climate Classification as a Diagnostic Tool for General Circulation Models." *Climate Research* 3:177–193. http://www.jstor.org/stable/24863394.

Lüdeke, M. K. B., P. H. Ramage, and G. H. Kohlmaier. 1996. "The Use of Satellite NDVI Data for the Validation of Global Vegetation Phenology Models: Application to the Frankfurt Biosphere Model." *Ecological Modelling* 91 (1–3): 255–270. https://doi.org/10.1016/0304-3800(95)00192-1.

Luo, M., F. Meng, C. Sa, Y. Duan, Y. Bao, T. Liu, and P. De Maeyer. 2021. "Response of Vegetation Phenology to Soil Moisture Dynamics in the Mongolian Plateau." *Catena* 206:105505. https://doi.org/10.1016/j.catena.2021.105505.

McDonough MacKenzie, C., A. S. Gallinat, and L. Zipf. 2020. "Low-Cost Observations and Experiments Return a High Value in Plant Phenology Research." *Applications in Plant Sciences* 8 (4): e11338. https://doi.org/10.1002/aps3.11338.

Melaas, E. K., M. A. Friedl, and Z. Zhu. 2013. "Detecting Interannual Variation in Deciduous Broadleaf Forest Phenology Using Landsat TM/ETM+ Data." *Remote Sensing of Environment* 132:176–185. https://doi.org/10.1016/j.rse.2013.01.011.

Meng, L., J. Mao, Y. Zhou, A. D. Richardson, X. Lee, P. E. Thornton, D. M. Ricciuto, et al. 2020. "Urban Warming Advances Spring Phenology but Reduces the Response of Phenology to Temperature in the Conterminous United States." *Proceedings of the National Academy of Sciences* 117 (8): 4228–4233. https://doi.org/10.1073/pnas.1911117117.

Migliavacca, M., M. Reichstein, A. D. Richardson, M. D. Mahecha, E. Cremonese, N. Delpierre, M. Galvagno, B. E. Law, G. Wohlfahrt, and T. Andrew Black. 2015. "Influence of Physiological Phenology on the Seasonal Pattern of Ecosystem Respiration in Deciduous Forests." *Global Change Biology* 21 (1): 363–376. https://doi.org/10.1111/gcb.12671.

Mohan, A. T., N. Lubbers, D. Livescu, and M. Chertkov. 2020. "EMbedding Hard Physical Constraints In Convolutional Neural Networks For 3D Turbulence." *ICLR 2020 Workshop on Integration of Deep Neural Models and Differential Equations*, Addis Ababa, Ethiopia.

Nguyen, L. H., D. R. Joshi, D. E. Clay, and G. M. Henebry. 2020. "Characterizing Land Cover/Land Use from Multiple Years of Landsat and MODIS Time Series: A Novel Approach Using Land Surface Phenology Modeling and Random Forest Classifier." *Remote Sensing of Environment* 238:111017. https://doi.org/10.1016/j.rse.2018.12.016.

Parihar, J., S. Goroshi, R. Singh, N. Krishnayya, M. Sirsayya, A. Kumar, L. Rawat, and A. Sonakia. 2013. "Observation of Forest Phenology Using Field-Based Digital Photography and Satellite Data." *Current Science*, 1740–1747. http://www.jstor.org/stable/24099757.

Park, D. S., E. A. Newman, and I. K. Breckheimer. 2021. "Scale Gaps in Landscape Phenology: Challenges and Opportunities." *Trends in Ecology & Evolution* 36 (8): 709–721. https://doi.org/10.1016/j.tree.2021.04.008.

Parsa, A. B., A. Movahedi, H. Taghipour, S. Derrible, and A. Mohammadian. 2020. "Toward Safer Highways, Application of XGBoost and SHAP for Real-Time Accident Detection and Feature Analysis." *Accident Analysis & Prevention* 136:105405. https://doi.org/10.1016/j.aap.2019.105405.

Peel, M. C., B. L. Finlayson, and T. A. McMahon. 2007. "Updated World Map of the Köppen-Geiger Climate Classification." *Hydrology and Earth System Sciences* 11 (5): 1633–1644. https://doi.org/10.5194/hess-11-1633-2007.

Peng, D., Y. Wang, G. Xian, A. R. Huete, W. Huang, M. Shen, F. Wang, et al. 2021. "Investigation of Land Surface Phenology Detections in Shrublands Using Multiple Scale Satellite Data." *Remote Sensing of Environment* 252:112133. https://doi.org/10.1016/j.rse.2020.112133.

Peng, D., X. Zhang, C. Wu, W. Huang, A. Gonsamo, A. R. Huete, K. Didan, B. Tan, X. Liu, and B. Zhang. 2017. "Intercomparison and Evaluation of Spring Phenology Products Using National Phenology Network and AmeriFlux Observations in the Contiguous United States." *Agricultural and Forest Meteorology* 242:33–46. https://doi.org/10.1016/j.agrformet.2017.04.009.

Piao, S., Q. Liu, A. Chen, I. A. Janssens, Y. Fu, J. Dai, L. Liu, X. Lian, M. Shen, and X. Zhu. 2019. "Plant Phenology and Global Climate Change: Current Progresses and Challenges." *Global Change Biology* 25 (6): 1922–1940. https://doi.org/10.1111/gcb.14619.

Prezhdo, O. V. 2020. "Advancing Physical Chemistry with Machine Learning." *The Journal of Physical Chemistry Letters* 11 (22): 9656–9658. https://doi.org/10.1021/acs.jpclett.0c03130.

Purdy, L. M., Z. Sang, E. Beaubien, and A. Hamann. 2023. "Validating Remotely Sensed Land Surface Phenology with Leaf Out Records from a Citizen Science Network."

International Journal of Applied Earth Observation Geoinformation 116:103148. https://doi.org/10.1016/j.jag.2022.103148.

Raissi, M., P. Perdikaris, and G. E. Karniadakis. 2019. "Physics-Informed Neural Networks: A Deep Learning Framework for Solving Forward and Inverse Problems Involving Nonlinear Partial Differential Equations." *Journal of Computational Physics* 378:686–707. https://doi.org/10.1016/j.jcp.2018.10.045.

Ren, Q., C. He, Q. Huang, and Y. Zhou. 2018. "Urbanization Impacts on Vegetation Phenology in China." *Remote Sens* 10:1905. https://doi.org/10.3390/rs10121905.

Richardson, A. D., T. F. Keenan, M. Migliavacca, Y. Ryu, O. Sonnentag, and M. Toomey. 2013. "Climate Change, Phenology, and Phenological Control of Vegetation Feedbacks to the Climate System." *Agricultural and Forest Meteorology* 169: 156–173. https://doi.org/10.1016/j.agrformet.2012.09.012.

Savitzky, A., and M. J. E. Golay. 1964. "Smoothing and Differentiation of Data by Simplified Least Squares Procedures." *Analytical Chemistry* 36 (8): 1627–1639. https://doi.org/10.1021/ac60214a047.

Seyednasrollah, B., A. M. Young, K. Hufkens, T. Milliman, M. A. Friedl, S. Frolking, and A. D. Richardson. 2019. "Tracking Vegetation Phenology Across Diverse Biomes Using Version 2.0 of the PhenoCam Dataset." *Scientific Data* 6 (1): 222. https://doi.org/10.1038/s41597-019-0229-9.

Shen, M., Y. Tang, J. Chen, X. Zhu, and Y. Zheng. 2011. "Influences of Temperature and Precipitation Before the Growing Season on Spring Phenology in Grasslands of the Central and Eastern Qinghai-Tibetan Plateau." *Agricultural and Forest Meteorology* 151 (12): 1711–1722. https://doi.org/10.1016/j.agrformet.2011.07.003.

Silveira, E. M. O., A. M. Pidgeon, M. Persche, and V. C. Radeloff. 2024. "Remotely-Sensed Phenoclusters of Wisconsin's Forests, Shrublands, and Grasslands for Biodiversity Applications." *Forest Ecology & Management* 561:121878. https://doi.org/10.1016/j.foreco.2024.121878.

Slack, D., S. Hilgard, E. Jia, S. Singh, and H. Lakkaraju. 2020. "Fooling LIME and SHAP: Adversarial Attacks on Post Hoc Explanation Methods." *Proceedings of the AAAI/ACM Conference on AI, Ethics, and Society. Presented at the AIES '20: AAAI/ACM Conference on AI, Ethics, and Society, ACM*, 180–186. New York NY USA. https://doi.org/10.1145/3375627.3375830.

Stöckli, R., T. Rutishauser, I. Baker, M. Liniger, and A. Denning. 2011. "A Global Reanalysis of Vegetation Phenology." *Journal of Geophysical Research* 116 (G3): 116. https://doi.org/10.1029/2010JG001545.

Sun, P., Y. Wu, J. Xiao, J. Hui, J. Hu, F. Zhao, L. Qiu, and S. Liu. 2019. "Remote Sensing and Modeling Fusion for Investigating the Ecosystem Water-Carbon Coupling Processes." *Science of the Total Environment* 697:134064. https://doi.org/10.1016/j.scitotenv.2019.134064.

Templ, B., E. Koch, K. Bolmgren, M. Ungersböck, A. Paul, H. Scheifinger, T. Rutishauser, et al. 2018. "Pan European Phenological Database (PEP725): A Single Point of Access

for European Data." *International Journal of Biometeorology* 62 (6): 1109–1113. https://doi.org/10.1007/s00484-018-1512-8.

Thornton, M. M., R. Shrestha, Y. Wei, P. E. Thornton, S. Kao, and B. E. Wilson. 2022. *Daymet: Daily Surface Weather Data on a 1-Km Grid for North America, Version 4*. ORNL DAAC, Oak Ridge, Tennessee, USA: Oak Ridge Tenn. USA Version 4. https://doi.org/10.3334/ORNLDAAC/2129.

Tian, F., Z. Cai, H. Jin, K. Hufkens, H. Scheifinger, T. Tagesson, B. Smets, et al. 2021. "Calibrating Vegetation Phenology from Sentinel-2 Using Eddy Covariance, PhenoCam, and PEP725 Networks Across Europe." *Remote Sensing of Environment* 260:112456. https://doi.org/10.1016/j.rse.2021.112456.

Tian, J., X. Luo, H. Xu, J. K. Green, H. Tang, J. Wu, and S. Piao. 2024. "Slower Changes in Vegetation Phenology Than Precipitation Seasonality in the Dry Tropics." *Global Change Biology* 30 (1): e17134. https://doi.org/10.1111/gcb.17134.

Touhami, I., H. Moutahir, D. Assoul, K. Bergaoui, H. Aouinti, J. Bellot, and J. M. Andreu. 2022. "Multi-Year Monitoring Land Surface Phenology in Relation to Climatic Variables Using MODIS-NDVI Time-Series in Mediterranean Forest, Northeast Tunisia." *Acta Oecologica* 114:103804. https://doi.org/10.1016/j.actao.2021.103804.

Tseng, K.-H., K. Chung-Yen, L. Min-Hui, C. Shum, M. M. Rahman, Y. Jia, Y. Ting-Yi, and P.-H. Shih. 2019. "Using MODIS/Terra and Landsat Imageries to Improve Surface Water Quantification in Sylhet, Bangladesh." *Terrestrial Atmospheric and Oceanic Sciences* 30 (1): 111–126. https://doi.org/10.3319/TAO.2018.11.15.04.

Turner, D. P., S. V. Ollinger, and J. S. Kimball. 2004. "Integrating Remote Sensing and Ecosystem Process Models for Landscape- to Regional-Scale Analysis of the Carbon Cycle." *BioScience* 54 (6): 573. https://doi.org/10.1641/0006-3568(2004)054[0573:IRSAEP]2.0.CO;2.

Vannest, K. J., R. I. Parker, J. L. Davis, D. A. Soares, and S. L. Smith. 2012. "The Theil–Sen Slope for High-Stakes Decisions from Progress Monitoring." *Behavioral Disorders* 37 (4): 271–280. https://doi.org/10.1177/019874291203700406.

Verhegghen, A., S. Bontemps, and P. Defourny. 2014. "A Global NDVI and EVI Reference Data Set for Land-Surface Phenology Using 13 Years of Daily SPOT-VEGETATION Observations." *International Journal of Remote Sensing* 35 (7): 2440–2471. https://doi.org/10.1080/01431161.2014.883105.

Vitasse, Y., F. Baumgarten, C. M. Zohner, T. Rutishauser, B. Pietragalla, R. Gehrig, J. Dai, H. Wang, Y. Aono, and T. H. Sparks. 2022. "Understanding Urban Plant Phenology for Sustainable Cities and Planet." *Nature Climate Change* 12 (4): 300–302. https://doi.org/10.1038/s41558-022-01283-y.

Wang, C., J. Chen, J. Wu, Y. Tang, P. Shi, T. A. Black, and K. Zhu. 2017. "A Snow-Free Vegetation Index for Improved Monitoring of Vegetation Spring Green-Up Date in Deciduous Ecosystems." *Remote Sensing of Environment* 196:1–12. https://doi.org/10.1016/j.rse.2017.04.031.

Wang, H., R. Magagi, K. Goïta, M. Trudel, H. McNairn, and J. Powers. 2019. "Crop Phenology Retrieval via Polarimetric

SAR Decomposition and Random Forest Algorithm." *Remote Sensing of Environment* 231:111234. https://doi.org/10.1016/j.rse.2019.111234.

Wang, J., X. Zhang, and K. Rodman. 2021. "Land Cover Composition, Climate, and Topography Drive Land Surface Phenology in a Recently Burned Landscape: An Application of Machine Learning in Phenological Modeling." *Agricultural and Forest Meteorology* 304–305:108432. https://doi.org/10.1016/j.agrformet.2021.108432.

Wang, L., H. J. De Boeck, L. Chen, C. Song, Z. Chen, S. McNulty, and Z. Zhang. 2022. "Urban Warming Increases the Temperature Sensitivity of Spring Vegetation Phenology at 292 Cities Across China." *Science of the Total Environment* 834:155154. https://doi.org/10.1016/j.scitotenv.2022.155154.

Wang, L., P. Wang, S. Liang, X. Qi, L. Li, and L. Xu. 2019. "Monitoring Maize Growth Conditions by Training a BP Neural Network with Remotely Sensed Vegetation Temperature Condition Index and Leaf Area Index." *Computers and Electronics in Agriculture* 160:82–90. https://doi.org/10.1016/j.compag.2019.03.017.

Wang, M., P. Li, C. Peng, J. Xiao, X. Zhou, Y. Luo, and C. Zhang. 2022. "Divergent Responses of Autumn Vegetation Phenology to Climate Extremes Over Northern Middle and High Latitudes." *Global Ecology Biogeography* 31 (11): 2281–2296. https://doi.org/10.1111/geb.13583.

Wang, M., J. Zhao, H. Zhang, Z. Zhang, X. Guo, T. Zhang, and R. Wu. 2023. "Detecting the Response Characteristics and Thresholds of Grassland Spring Phenology to Climatic Factors in the Mongolian Plateau." *Ecological Indicators* 153:110440. https://doi.org/10.1016/j.ecolind.2023.110440.

Wang, N., P. Yang, J. G. P. W. Clevers, S. Wieneke, and L. Kooistra. 2023. "Decoupling Physiological and Non-Physiological Responses of Sugar Beet to Water Stress from Sun-Induced Chlorophyll Fluorescence." *Remote Sensing of Environment* 286:113445. https://doi.org/10.1016/j.rse.2022.113445.

Wilcox, R. 1998. "A Note on the Theil-Sen Regression Estimator When the Regressor is Random and the Error Term is Heteroscedastic." *Biometrical Journal* 40 (3): 261–268. https://doi.org/10.1002/(SICI)1521-4036(199807)40:3<261::AID-BIMJ261>3.0.CO;2-V.

Willmott, C. J., S. G. Ackleson, R. E. Davis, J. J. Feddema, K. M. Klink, D. R. Legates, J. O'Donnell, and C. M. Rowe. 1985. "Statistics for the Evaluation and Comparison of Models." *Journal of Geophysical Research Oceans* 90 (C5): 8995–9005. https://doi.org/10.1029/JC090iC05p08995.

Wu, C., A. Gonsamo, C. M. Gough, J. M. Chen, and S. Xu. 2014. "Modeling Growing Season Phenology in North American Forests Using Seasonal Mean Vegetation Indices from MODIS. Remote Sens." *Remote Sensing of Environment* 147:79–88. https://doi.org/10.1016/j.rse.2014.03.001.

Wu, S., J. Wang, Z. Yan, G. Song, Y. Chen, Q. Ma, M. Deng, et al. 2021. "Monitoring Tree-Crown Scale Autumn Leaf Phenology in a Temperate Forest with an Integration of PlanetScope and Drone Remote Sensing Observations." *Isprs Journal of Photogrammetry & Remote Sensing* 171:36–48. https://doi.org/10.1016/j.isprsjprs.2020.10.017.

Wu, W., Y. Sun, K. Xiao, and Q. Xin. 2021. "Development of a Global Annual Land Surface Phenology Dataset for 1982–2018 from the AVHRR Data by Implementing Multiple Phenology Retrieving Methods." *International Journal of Applied Earth Observation Geoinformation* 103:102487. https://doi.org/10.1016/j.jag.2021.102487.

Xie, Q., C. E. Moore, J. Cleverly, C. C. Hall, Y. Ding, X. Ma, A. Leigh, and A. Huete. 2023. "Land Surface Phenology Indicators Retrieved Across Diverse Ecosystems Using a Modified Threshold Algorithm." *Ecological Indicators* 147:110000. https://doi.org/10.1016/j.ecolind.2023.110000.

Xin, Q., J. Li, Z. Li, Y. Li, and X. Zhou. 2020. "Evaluations and Comparisons of Rule-Based and Machine-Learning-Based Methods to Retrieve Satellite-Based Vegetation Phenology Using MODIS and USA National Phenology Network Data." *International Journal of Applied Earth Observation Geoinformation* 93:102189. https://doi.org/10.1016/j.jag.2020.102189.

Yan, X., Y. Guo, Y. Zhang, J. Chen, Y. Jiang, C. Zuo, W. Zhao, and W. Shi. 2024. "Combining Physical Mechanisms and Deep Learning Models for Hourly Surface Ozone Retrieval in China." *Journal of Environmental Management* 351:119942. https://doi.org/10.1016/j.jenvman.2023.119942.

Yang, X., J. Wu, X. Chen, P. Ciais, F. Maignan, W. Yuan, S. Piao, et al. 2021. "A Comprehensive Framework for Seasonal Controls of Leaf Abscission and Productivity in Evergreen Broadleaved Tropical and Subtropical Forests." *The Innovation* 2 (4): 100154. https://doi.org/10.1016/j.xinn.2021.100154.

Yue, S., and C. Y. Wang. 2002. "Applicability of Prewhitening to Eliminate the Influence of Serial Correlation on the Mann-Kendall Test." *Water Resources Research* 38 (6): 4–1–4–7. https://doi.org/10.1029/2001WR000861.

Zang, Y., Z. Yu, K. Xu, X. Lan, M. Chen, S. Yang, and H. Chen. 2021. "Principle-Driven Fiber Transmission Model Based on PINN Neural Network." *Journal of Lightwave Technology* 40 (2): 404–414. https://doi.org/10.1109/JLT.2021.3139377.

Zeng, L., B. D. Wardlow, D. Xiang, S. Hu, and D. Li. 2020. "A Review of Vegetation Phenological Metrics Extraction Using Time-Series, Multispectral Satellite Data." *Remote Sensing of Environment* 237:111511. https://doi.org/10.1016/j.rse.2019.111511.

Zhang, G., H. Ma, S. Liang, A. Jia, T. He, and D. Wang. 2022. "A Machine Learning Method Trained by Radiative Transfer Model Inversion for Generating Seven Global Land and Atmospheric Estimates from VIIRS Top-Of-Atmosphere Observations." *Remote Sensing of Environment* 279:113132. https://doi.org/10.1016/j.rse.2022.113132.

Zhang, J., J. Xiao, X. Tong, J. Zhang, P. Meng, J. Li, P. Liu, and P. Yu. 2022. "NIRv and SIF Better Estimate Phenology Than NDVI and EVI: Effects of Spring and Autumn Phenology on Ecosystem Production of Planted Forests." *Agricultural and Forest Meteorology* 315:108819. https://doi.org/10.1016/j.agrformet.2022.108819.

Zhang, X., M. A. Friedl, C. B. Schaaf, and A. H. Strahler. 2004. "Climate Controls on Vegetation Phenological Patterns in Northern Mid-And High Latitudes Inferred from MODIS Data." *Global Change Biology* 10 (7): 1133–1145. https://doi.org/10.1111/j.1529-8817.2003.00784.x.

Zhang, X., M. A. Friedl, C. B. Schaaf, A. H. Strahler, J. C. F. Hodges, F. Gao, B. C. Reed, and A. Huete. 2003. "Monitoring Vegetation Phenology Using MODIS. Remote Sens." *Remote Sensing of Environment* 84 (3): 471–475. https://doi.org/10.1016/S0034-4257(02)00135-9.

Zhao, B., A. Donnelly, and M. D. Schwartz. 2020. "Evaluating Autumn Phenology Derived from Field Observations, Satellite Data, and Carbon Flux Measurements in a Northern Mixed Forest, USA." *International Journal of Biometeorology* 64 (5): 713–727. https://doi.org/10.1007/s00484-020-01861-9.

Zhou, D., S. Zhao, L. Zhang, and S. Liu. 2016. "Remotely Sensed Assessment of Urbanization Effects on Vegetation Phenology in China's 32 Major Cities." *Remote Sensing of Environment* 176:272–281. https://doi.org/10.1016/j.rse.2016.02.010.

Zhou, J., M. J. Deitch, S. Grunwald, and E. Screaton. 2023. "Do the Mann-Kendall Test and Theil-Sen Slope Fail to Inform Trend Significance and Magnitude in Hydrology?" *Hydrological Sciences Journal* 68 (9): 1241–1249. https://doi.org/10.1080/02626667.2023.2212166.

Zhou, L., W. Zhou, J. Chen, X. Xu, Y. Wang, J. Zhuang, and Y. Chi. 2022. "Land Surface Phenology Detections from Multi-Source Remote Sensing Indices Capturing Canopy Photosynthesis Phenology Across Major Land Cover Types in the Northern Hemisphere." *Ecological Indicators* 135:108579. https://doi.org/10.1016/j.ecolind.2022.108579.

Zhou, X., Q. Xin, Y. Dai, and W. Li. 2021. "A Deep-Learning-Based Experiment for Benchmarking the Performance of Global Terrestrial Vegetation Phenology Models." *Global Ecology & Biogeography* 30 (11): 2178–2199. https://doi.org/10.1111/geb.13374.

Zhu, Z., and C. E. Woodcock. 2014. "Continuous Change Detection and Classification of Land Cover Using All Available Landsat Data." *Remote Sensing of Environment* 144:152–171. https://doi.org/10.1016/j.rse.2014.01.011.

Appendixes
Appendix A

Supplementary materials for the Table SA1 and Table SA2 are available at https://drive.google.com/drive/folders/1ImCKGMLXkUTgHgyM3fyN2YnU2EpbTKl-?usp=sharing.

Table A3. The field observed vegetation classification and satellite remote sensing vegetation classification were used in this study.

| PhenoCam	USA-NPN	MODIS	Abbreviations
evergreen broadleaf; evergreen needleleaf	evergreen broadleaf, evergreen conifer, semi-evergreen broadleaf, evergreen forb	evergreen needleleaf forests; evergreen broadleaf forests	EV (evergreen vegetation)
deciduous broadleaf; deciduous needleleaf	deciduous broadleaf; deciduous conifer	deciduous needleleaf forests; deciduous broadleaf forests	DV (deciduous vegetation)
shrubs; mixed vegetation	shrub forest	mixed forests; closed shrublands; open shrublands;	SF (shrub forests)
tundra	drought deciduous broadleaf; graminoid	woody savannas; savannas	SDV (stressed deciduous vegetation)

Appendix B
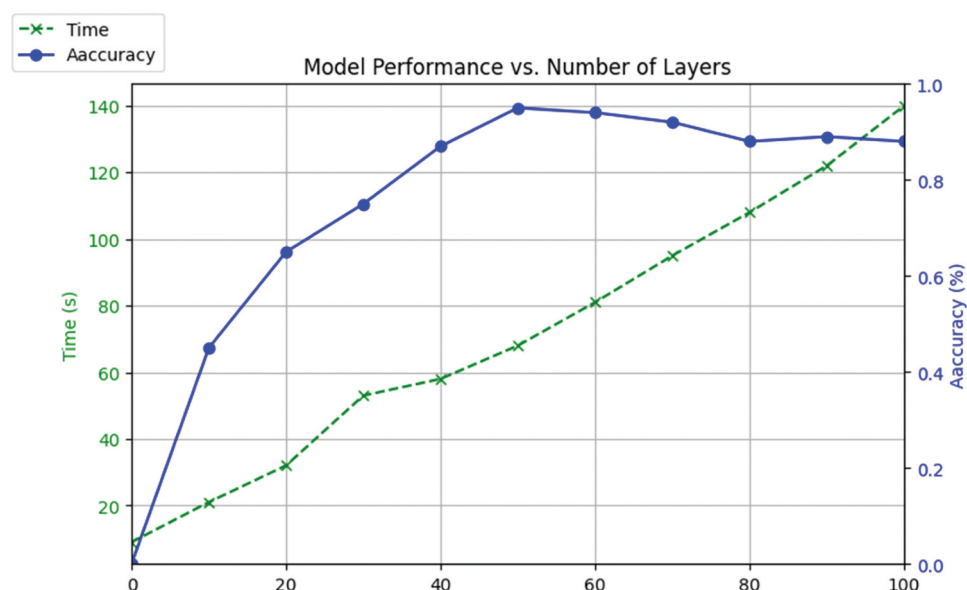
Figure B1. Impact of layers on the computational efficiency and predictive accuracy of the model.

Appendix C

To analyze the performance of the model, we also evaluated and compared the overall performance of the model on all datasets. The results are summarized in the following tables and discussed in detail below. According to the results in Table C1 and Table C2, each model performs differently on four evaluation metrics.

Table C1 illustrates the performance metrics of the SOS for each model across the four evaluation datasets. The PCNNs model demonstrates the highest overall performance among all the models tested, with an MBE error of 8.35 days. This indicates its ability to make predictions that closely align with actual observations. Among the four vegetation types, the DV vegetation type exhibits the highest prediction accuracy with RMSE and MAE of 5.71 days and 4.06 days, respectively. This accuracy surpassed the second-best performing EV vegetation type by 6.52 days. Specifically, the PCNNs method achieved superior accuracy, with an error of 4.06 days for SOS and 0.73 for WIA. The RMSE result of SDV vegetation type was the lowest among all methods, such as 28.52 days for SDV predicted by AT method. While the ANN method in SDV vegetation type predicted the lowest RMSE error with 19.86 days in the study region. Additionally, the SF vegetation type had a poor MBE result, with an error of 29.89 days for the AT method. The RF and ANN models showed comparable performance with a systematic bias of 0.61, but a smaller systematic bias compared to PCNNs model (WIA of 0.68). In comparison to machine

Table C1. The evaluation of SOS involves statistical analysis conducted on metrics derived from five satellite-based phenology retrieval methods. This assessment utilizes the MODIS product and incorporates data obtained from the USA-NPN.

	EV			DV			SF			SDV			Overall		
	RMSE (days)	MBE (days)	WIA	RMSE (days)	MBE (days)	WIA	RMSE (days)	MBE (days)	WIA	RMSE (days)	MBE (days)	WIA	RMSE (days)	MBE (days)	WIA
AT	18.22	12.44	0.57	8.01	11.14	0.58	14.62	29.89	0.56	28.52	21.6	0.57	12.5	21.36	0.57
CCR	18.71	16.71	0.58	7.96	9.53	0.62	17.73	27.83	0.58	24.44	24.17	0.51	20.5	19.51	0.59
RF	17.51	17.21	0.61	8.43	6.74	0.63	18.57	20.35	0.59	23.21	14.18	0.61	9.45	14.94	0.61
ANN	13.17	14.92	0.64	6.91	5.31	0.64	15.21	22.5	0.6	**19.86**	12.45	0.58	10.99	17.41	0.62
PCNNs	**12.23**	**11.42**	**0.67**	**5.71**	**4.06**	**0.73**	**13.28**	**18.23**	**0.63**	20.53	**11.39**	**0.63**	**8.35**	**12.37**	**0.68**

Table C2. The evaluation of the EOS involves statistical analysis conducted on metrics derived from six satellite-based phenology retrieval methods. These metrics are obtained by utilizing data from the USA-NPN.

	EV			DV			SF			SDV			Overall		
	RMSE (days)	MBE (days)	WIA	RMSE (days)	MBE (days)	WIA	RMSE (days)	MBE (days)	WIA	RMSE (days)	MBE (days)	WIA	RMSE (days)	MBE (days)	WIA
AT	23.34	**6.87**	0.61	12.33	10.8	0.71	22.45	21.07	0.61	17.57	27.75	0.68	16.7	−16.57	0.67
CCR	18.27	7.83	0.68	11.62	7.37	0.74	26.28	−26.4	0.66	19.86	21.55	0.51	16.8	18.99	0.63
RF	13.27	13.81	0.73	9.81	3.15	0.73	18.37	16.48	0.71	**12.35**	22.34	0.73	13.35	12.21	**0.71**
ANN	12.82	11.42	0.72	9.46	−5.22	0.76	13.91	−12.3	0.68	14.38	21.75	0.71	17.38	11.84	0.69
PCNNs	**12.31**	10.69	**0.74**	**8.91**	**2.35**	**0.78**	**11.05**	11.51	**0.75**	12.39	**19.17**	**0.78**	14.51	**9.79**	**0.71**

learning methods, the AT method and CCR method generally display inferior prediction results, with an approximately 5 days difference in overall performance.

From Table C2, the PCNNs model provides the most accurate and reliable predictions across all datasets, with results indicating a predicted bias of 9.79 days and a systematic error of 0.71 (WIA). The AT model shows a favorable MBE (6.87 days) result for the EV vegetation type, while its predictions exhibit a large scatter (WIA of 0.61). Among the four vegetation types predicted by EOS, DV shows the best prediction results with an MBE error of 2.35 days. The SF and SDV predictions yielded relatively inferior results, with errors of more than about 20 days on the AT and CCR methods. It is worth noting that three machine learning methods (RF, ANN, and PCNNs) performed comparably with a small systematic bias of approximately 0.7. The RF model achieved the smallest error of 12.35 days in the RMSE results for the SDV vegetation type. Combining the PCNNs methods in Tables C1 and C2, the advantage of the PCNNs approach was particularly pronounced in the prediction of EOS (RMSE of 11.05 days) than SOS (RMSE of 13.28 days) for SF vegetation types.

Figure C3 depicts the relationship between various phenological stages and six meteorological variables, where the red color represents a robust positive correlation, and blue color represents a strong negative correlation. The results show that there are significant differences in the intricate correlation patterns between different vegetation phenological phases and meteorological variables, highlighting the importance of the influence of different meteorological factors on vegetation phenology across different vegetation types. Specifically, three distinct phenological stages of vegetation exhibit a robust positive correlation with daylength, approaching a correlation coefficient of 1.0 in the central and eastern regions. Compared with the other four meteorological variables, the correlation between maximum air temperature and precipitation varies greatly between SOS and EOS. Precipitation and maximum air temperature are negatively correlated at SOS mainly for EV and SDV vegetation types, with correlation coefficients of −0.8 and −0.4, respectively, whereas the correlation coefficients of maximum air temperature and precipitation at EOS are 0.7 and 0.5, respectively. In the DV region, SOS and EOS show strong correlations with precipitation of −0.8 and 0.7, respectively. This result suggests that precipitation has substantial negative and positive effects on the timing of vegetation growth and senescence processes in this region. Moreover, both DV and SDV vegetation types exhibit strong correlations with radiation in their phenological patterns, locally exceeding a correlation coefficient of 0.6. Compared with other meteorological variables, the correlation between daylength and vegetation phenology shows generally strong and mostly positive in vegetated areas with positive correlation as high as 0.9 and negative correlation at −0.8. In contrast, vegetation phenology displays more subtle variations in its correlation with minimum air temperature (−0.1), radiation (0.2) and water vapor (−0.3) in the northwest region.
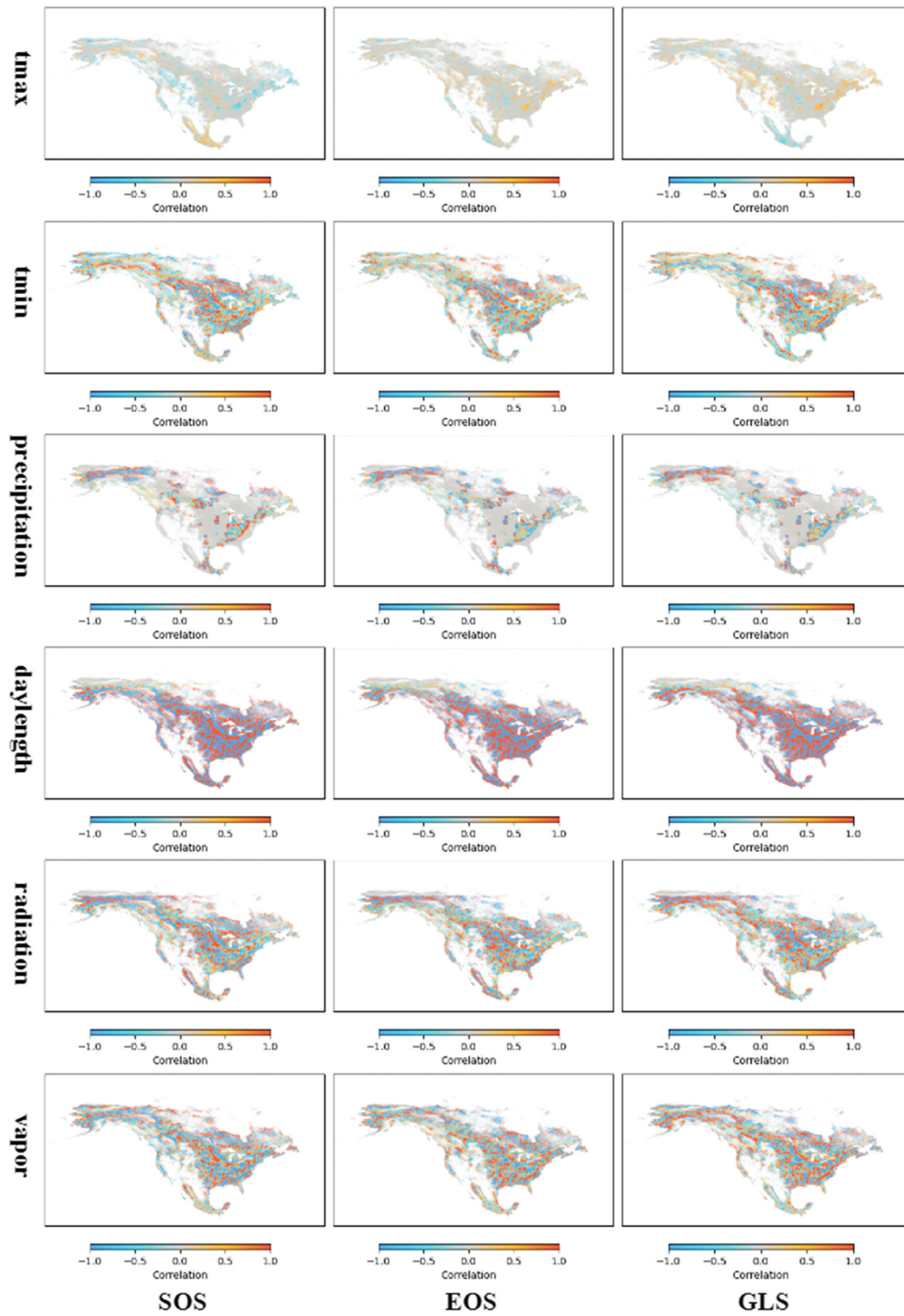
Figure C3. Correlations of six meteorological variables with the mean vegetation phenology from 2001 to 2021. The tmax and tmin denote the maximum air temperature and minimum air temperature, respectively.